Article:

Wynn, Alasdair, Lipschultz, Bruce orcid.org/0000-0001-5968-3684, Cziegler, Istvan orcid.org/0000-0003-1040-8918 et al. (15 more authors) (2018) Investigation into the formation of the scrape-off layer density shoulder in JET ITER-like wall L-mode and H-mode plasmas. Nuclear Fusion. 056001. pp. 1-22. ISSN 1741-4326

https://doi.org/10.1088/1741-4326/aaad78

Investigation of the Scrape-off layer density shoulder formation in JET ITER-like wall L-mode and H-mode plasmas

A. Wynn[a], B. Lipschultz[a**], I. Cziegler[a], J. Harrison[b], A. Jaervinen[c] G. F. Matthews[b], J. Schmitz[a,d], B.Tal[e], M. Brix[b], C. Guillemaut[b,f], D. Frigione[g], A. Huber[d], E. Joffrin[h], U. Kruzei[b], F. Militello[b], A. Nielsen[i], N.R. Walkden[b], S. Wiesen[d] and JET contributors*

EUROfusion Consortium, JET, Culham Science Centre, Abingdon, OX14 3DB, UK

[a]York Plasma Institute, University of York, Heslington, York, YO10 5DD, UK
[b]CCFE ,Culham Science Centre, Abingdon, OX14 3DB, UK
[c]Lawrence Livermore National Laboratory, Livermore, California, USA
[d]Forschungszentrum Jülich Gmbh, Institut für Energie- und Klimaforschung - Plasmaphysik, 52425 Jülich, Germany
[e]Wigner Research Centre for Physics, HAS, P.O.B. 49, H - 1525 Budapest, Hungary
[f]Instituto de Plasmas e Fusao Nuclear, Universidade Lisboa, Portugal
[g]Associazione EURATOM-ENEA sulla Fusione, CP 65, Frascati, Rome, Italy
[h]Association EURATOM-CEA, CEA/DSM/DRFC CEA-Cadarache, 13108 Saint Paul Lez Durance, France
[i]Association Euratom DTU, Technical University of Denmark, PO Box 49, DK 4000 Roskilde, Denmark
*See the author list of X. Litaudon et al 2017 Nucl. Fusion 57 102001
**Corresponding author e-mail: bruce.lipschultz@york.ac.uk

Abstract: The low temperature boundary layer plasma (Scrape-Off-Layer or SOL) between the hot core and the surrounding vessel determines the level of power-loading, erosion and implantation of material surfaces, and thus the viability of tokamak-based fusion as an energy source. This study explores mechanisms affecting the formation of flattened density profiles, so-called 'density shoulders', in the low-field side (LFS) SOL, which modify ion and neutral fluxes to surfaces – and subsequent erosion. We find that increases in SOL parallel resistivity, Λ_{div} ($=[L_{||}\nu_{ei}\Omega_i]/c_s\Omega_e$), postulated to lead to shoulder growth through changes in SOL turbulence characteristics, correlates with increases in SOL shoulder amplitude, A_s, only under a subset of conditions (D_2-fuelled L-mode density scans with outer strike point on the horizontal target). Λ_{div} fails to correlate with A_s for cases of N_2 seeding or during sweeping of the strike point across the horizontal target. The limited correlation of Λ_{div} and A_s is also found for H-mode discharges. Thus, while Λ_{div} above a threshold of ~1 may be necessary for shoulder formation and/or growth, another mechanism is required. More significantly we find that in contrast to parallel resistivity, outer divertor recycling, as quantified by the total outer divertor Balmer D_α emission, I-D_α, does scale with A_s where Λ_{div} does and even where Λ_{div} fails. Divertor recycling *could* lead to SOL density shoulder formation through: a) reducing the parallel to the field flow (loss) of ions out of the SOL to the divertor; and b) changes in radial electric fields which lead to ExB poloidal flows

as well as potentially affecting SOL turbulence birth characteristics. Thus changes in divertor recycling may be the sole process in bringing about SOL density shoulders or in tandem with parallel resistivity.

1. Introduction

Understanding the physics governing the intensity and nature of plasma interactions with vessel surfaces is critical to the attainment of fusion power in magnetically controlled devices. By design, next step fusion devices such as ITER, and likely future devices such as DEMO, will prevent the hot, fusing, confined plasma from directly contacting the vessel surfaces by using a divertor magnetic geometry ([1] and references therein). In an ideal divertor scenario, all of the energy and particles exiting the edge of the confined region, through what is known as the last closed flux surface (LCFS) or separatrix, are transported to the divertor region. This ideal generally holds for energy transport due to the dominance of energy transport parallel to magnetic field lines compared to the perpendicular direction, leading to high divertor power flux densities for attached H-mode plasmas [2]. Techniques have been developed to mitigate those high power fluxes by inducing divertor detachment [3, 4].

A number of studies have shown that there are still significant charge exchange neutral and anomalous cross-field ion fluxes to main chamber surfaces outside the divertor region [5-8]. Indeed, under detached divertor conditions, the divertor ion (and power) fluxes have been strongly reduced leaving the total ion flux to main chamber surfaces comparable to that to the divertor in both L-mode and H-mode plasmas [9]. Due to the large area of the main chamber walls the steady state ion and neutral heat flux densities there are small compared to the divertor.

The main causes of erosion to plasma facing components (PFCs, typically limiters) are sputtering by a) radial ion fluxes; and b) the flux of high energy CX neutrals that are born inside the separatrix [10, 11]. For each sputtering erosion source the shape of the density profile and the mechanisms that control it are central. For example, when the scale length of the density gradient near main chamber surfaces (‘far SOL’) becomes large, often described as ‘shoulder’ formation’ [7, 12], the ion density at the limiter increases and the ion fluxes ($\propto nC_s$) to such surfaces rise strongly. (Herein we use the term ‘shoulder’ interchangeably with ‘density shoulder’ in the low-field side SOL).

Shoulder formation and the resultant flattening of the far SOL density profile have been found to occur in several tokamaks in a variety of operating regimes [7-9, 12-17]. The initial observations by McCormick showed that the flattening in the far SOL occurred at high density and low current [12]. LaBombard [7] first coined the description of the ‘near’ and ‘far’ SOL. We use the following definition for the dividing line between the two regions - “ The location of the ‘breakpoint’ between the region of short e-folding length near the separatrix (‘near’ SOL) and longer e-folding length (‘far’ SOL)”[13] corresponding to the shoulder. As the operating densities of such plasmas approached the global density limit [18], the flattened region moved towards the separatrix (sometimes called ‘broadening’).

Previous research into SOL cross-field transport showed that the flattened SOL density profiles are not consistent with diffusive transport, and that advection is the likely transport mechanism [7, 9, 13, 19-21]. Boedo [21] showed that turbulence accounted for up to 50% of the radial transport onto main chamber surfaces. LaBombard [22] found that flattening SOL density profiles correlated with larger amplitude fluctuations in the SOL as the core plasma density was increased on C-Mod. This relationship has been confirmed on a number of tokamaks including TCV [23], DIII-D [8], and MAST [24].

Despite the well-documented correlation, only recently have code and analytic models been advanced that appear to predict the statistical properties of SOL advection and the resultant time averaged density profiles [25, 26].

Both experimental measurements and models show that advective transport is manifested as filamentary structures in the SOL [27] elongated along magnetic field lines, with lengths on the order of πqR(~10m), and narrow perpendicular to it, of order 5-10ρ_i (1-2cm, larger in spherical tokamaks[28]). Here, q is the safety factor, R is the major radius and ρ_i is the ion gyro-radius. Filaments travel both radially and poloidally at velocities in the range 500-1000m/s.

A common conjecture is that the effective electrical resistances both parallel and perpendicular to the magnetic field line within a filament influence its characteristics [29]. More specifically, the electrical disconnection from the divertor target sheath, occurring at high collisionality (so-called ‘inertial regime’), has been correlated to changes in filament characteristics (relation existing between size and velocity), and thus changes in advective transport [23, 30-32]. An expression of the divertor collisionality/resistance is given by [30]

$$\Lambda_{div} = \frac{L_{\parallel}\nu_{ei}\Omega_i}{c_s\Omega_e} = 3.4x10^{-19}\frac{L_{\parallel}n_e\Omega_i}{T_e^2} \qquad (1)$$

where ν_{ei} is the electron-ion collision frequency, $L_{//}$ (m) is the magnetic connection length from the LFS (low-field side) mid-plane of the plasma to the divertor target, Ω_i(s^{-1}) and Ω_e(s^{-1}) are the gyro-frequency of ions and electrons respectively, c_s (m/s) is the sound speed, n_e (m^{-3}) is the electron density and T_e (eV) is the electron temperature.

The experimental correlation between increased SOL density profile flattening, increases in filament size and velocity and Λ_{div}, was demonstrated by Carralero [32] for ASDEX-Upgrade (outer divertor strike point on the vertical target) and JET (outer divertor strike point on the horizontal target (tile 5)) L-mode plasmas. Carralero found that increasing Λ_{div} past 1 and divertor detachment[16], using either D_2 fuelling or N_2 seeding[32], led to further flattening of the SOL profile as evidenced by an increase in the effective density e-folding length, λ_n, averaged over a region in the upstream SOL. Expansion of the far SOL flattened region *toward* the separatrix was found for ASDEX-Upgrade as Λ_{div} was increased further. The concurrent increase in both the filament size and velocity, shown only for the case of D_2 fuelling, was proposed as the causal mechanism for SOL flattening and increase in radial flux. Vianello states that a 'high level of Λ_{div} is found to be a necessary but not sufficient condition in order to obtain a flatter density profile'.

The strong correlation between filament characteristics changes and shoulder formation in ASDEX-Upgrade L-mode vertical target plasmas is not universally found. Vianello [33], in studying turbulent transport in TCV L-mode, D_2 fuelled plasmas with an open, or horizontal target divertor, found that λ_n does *not* correlate strongly with Λ_{div} , nor is there a sudden increase in λ_n when Λ_{div} increases past 1 in all cases. Furthermore, flattened LFS SOL profiles (shoulders) were also observed at low Λ_{div}. The TCV work is also notable in that Λ_{div} was varied through both density and connection length scans.

More recent research with H-mode plasmas by Carralero et al also comes to the conclusion that Λ_{div} above some threshold may be necessary but not sufficient to lead to shoulder growth[34, 35]. In addition, values of λ_n and filament size no longer display a sharp increase at $\Lambda_{div} \sim 1$. Ionization and charge exchange near the limiter are proposed as a second mechanism, interacting with the Λ_{div} effect on filament properties, to lead to shoulder growth.

The motion of turbulent filaments has been extensively characterized numerically. Significant progress has been made in modelling filaments, initiating from 2D slab geometries, extending to 3D slabs [26, 36, 37] and also tokamak relevant geometries [38, 39]. Direct comparisons between simulations and experiments have also been performed [40-42]. Recently, neutrals have been included self-consistently in tokamak relevant turbulence simulations in limited configuration [43]; implementation of x-point geometry is in progress.

The goal of the study presented in this paper is to examine various mechanisms that could lead to shoulder formation in the JET tokamak with the ITER-like Wall (ILW) where the main chamber limiter surfaces are Be and the divertor surfaces are tungsten[44]. We address these mechanisms without a direct measurement of turbulent filament properties. The focus is on the characteristics of the divertor and SOL that, if important, should be evident and correlated with shoulder formation and growth – e.g. as Λ_{div} is used in previous studies. The LFS SOL density shoulder formation mechanisms addressed in this paper are as follows:

(a) The conditions at, or inside, the separatrix (n_e, T_e and gradients) modifying SOL cross-field or radial transport (e.g. turbulent filament birth characteristics such as filament size, frequency, velocity…) and thus shoulders in the far SOL.

(b) That changes in parallel resistivity, quantified by divertor resistance (Λ_{div}) are changing upstream SOL radial transport as described in the Introduction (e.g. through changing filament characteristics as it travels through the SOL).

(c) Changes in local particle sources (e.g. ionization in the main chamber), which increase/decrease the local SOL density or

(d) Changes to sinks (e.g. parallel loss of ions along B to the divertor) could raise or lower the local density.

Similar discussions of the above mechanisms have appeared elsewhere [13, 26, 34, 45, 46].

Based on the results presented in this paper we find that mechanisms (a) – (c) are, individually, not sufficient to cause the formation of the SOL density shoulder.

More specifically, for (a) and (c), comparisons of discharges with the outer strike point located on the horizontal vs vertical target indicate that under the same core/separatrix conditions and main chamber neutral pressures, there is *no* shoulder formation for the vertical (closed) target operation, while there *are* shoulders formed for horizontal (open) target operation. *Thus mechanisms (a) and (c) are unlikely.*

Turning to the correlation of parallel resistivity with the upstream SOL density profile (mechanism b) we find that increases in $\boldsymbol{\Lambda}_{div}$ *are not sufficient* to predict or form a shoulder; whereas increases in $\boldsymbol{\Lambda}_{div}$ do correlate with increases in A_s under a subset of conditions (D_2-fueled L-mode density scans with outer strike point on the horizontal target), the same variation in $\boldsymbol{\Lambda}_{div}$ driven by N_2 seeding or D_2 fuelling with the vertical target has essentially no effect on upstream shoulder amplitude. Furthermore, we have also observed during sweeping the outer horizontal target strike point in major radius that significant changes in shoulder amplitude can occur *without any* change in Λ_{div}. *Thus, if parallel resistivity is related to shoulder formation at all it must be in tandem with another mechanism.*

The above assessment of the lack of consistent correlation between $\boldsymbol{\Lambda}_{div}$ and A_s extends to inter-ELM H-mode periods utilizing the horizontal target.

In comparison to parallel resistivity ($\boldsymbol{\Lambda}_{div}$), increases in divertor recycling, as quantified through the total outer divertor Balmer D_α line emission magnitude, I-D_α, and D_α emission profile width, *do* increase with upstream shoulder amplitude under D_2 fuelling and *do not* increase with N_2 seeding. We point to ion-neutral interactions of the fuel species (using D_α as a proxy) as potentially decreasing parallel ion flows (losses of ions) out of the upstream SOL or changing the radial electric field (mechanism d).

In summary of our judgment of shoulder formation mechanisms, we can agree with previous work [33, 35] that parallel resistivity cannot be the sole mechanism for shoulder formation (may be necessary but not sufficient). However, unlike Carralero [35], *the second mechanism appears related to divertor recycling as quantified through I-*D_α *for attached plasmas. It may be possible that divertor recycling is even a necessary and sufficient mechanism for shoulder formation.*

This paper is structured as follows. In section 2 the experimental setup is presented. Section 3 introduces basic quantitative measures of the SOL density shoulder characteristics and the effect of plasma current on the density profile. In section 4 the validity of $\boldsymbol{\Lambda}_{\rm div}$ as a general control parameter for the SOL density profile is investigated. In section 5 the role of mid-plane neutrals as an ion source is presented. In section 6, we present evidence that plasma-neutral interaction of the fuel species in the divertor region, indicated by the total outer divertor D_α emission, is a more general correlator for SOL density profile changes than $\boldsymbol{\Lambda}_{\rm div}$. In section 7, a brief study of H-modes is presented including the effect of D_2 fuelling and N_2 seeding. Sections 8 and 9 discuss and summarize the primary results of the study.

2. Experimental Setup

2.1 Diagnostics

Figure 1 shows a poloidal cross-section of JET-ILW with the different horizontal (open or HT, on tile 5) and vertical (closed or VT, on tile 7) outer target magnetic configurations and relevant diagnostics. For clarity, a close up of the divertor region is shown in figure 2.

The measurement of the SOL density profile is central to this study and the JET Li beam diagnostic [47] provides absolutely calibrated density profiles from approximately the pedestal top to the limiter radius. The Li beam enters the upper half of the plasma as shown in figure 1. When mapped to the midplane along flux surfaces to compare with other measurements, the midplane spatial resolution is ~2.5mm. Profiles are provided with a time resolution of 10 ms. In most cases the Li beam density profiles are averaged over 100ms.

A Penning–type gauge is substantially recessed from the vessel leading to poor time response (we estimate ~ 1 second), but provides the best currently available measurement of pressure at the midplane.

Divertor Langmuir probes (DLPs) provided target profiles of J_{sat}, n_e and T_e measurements across divertor surfaces at 100Hz, while J_{sat} was also available at 100 kHz. In L-mode cases, strike point sweeping of 4Hz and 1Hz frequency, in HT and VT respectively, with an amplitude of ~2.5cm, was used to provide fully resolved profiles of plasma characteristics across the divertor. However, not all probes on the HT were functional for the discharges in this study. That leads to data missing over sections of the divertor profile. Strike point sweeping was not used for H-mode cases.

Several gas injection locations were used for L-mode plasmas: GIM 11 (see figure 2) was always used for D_2 injection into the private flux region (PFR). However, GIM 9 moves from the common to private flux regions of the divertor plasma in shifting the equilibrium from HT to VT. The gas injected through GIM 9 was normally D_2 except for N_2 seeded discharges where the gas was switched to N_2. GIM 10 injects into the common flux region in all cases.

In the case of H-mode plasmas GIMs 10 and 11 were used for D_2 injection while GIM 9 was used for N_2 seeding.

Optical cameras, filtered for emission lines including D_α, were also employed for both upstream SOL and divertor measurements of local D_α emissivity (through inversions of brightness images) in 1D (upstream SOL) and 2D in the divertor [48] respectively. For upstream SOL inversions, figure 1 shows the location of the radial D_α emissivity measurement points, which are a subset of data from the main chamber viewing 1000x1000 pixel CCD camera (80 degree field of view) system ('KL1 system'). Lines of sight tangential to flux surfaces at a fixed Z were selected by mapping pixel locations to vessel structures[49]. This brightness profile is then Abel inverted to provide a D_α emissivity profile which, when multiplied by the S/XB coefficient, gives the local ionization source, S_{ion}. The S/XB coefficient is taken from ADAS [50] and is dependent on the local T_e and n_e. The S/XB coefficient has not been modified to take into account molecules. SOL T_e measurements are not available in JET which led us to assume an exponential profile starting at 100eV at the separatrix, based on power balance and Thomson measurements. The assumed T_e decay length (2 cm) across the SOL and T_e at the limiter radius (10 eV) are based on past scanning Langmuir probe measurements from similar pulses. The sensitivity of the derived ionization rate to the above assumptions is small compared to D_α emissivity uncertainties; the S/XB coefficients for interpreting the local D_α emissivity as an ionization rate are not sensitive to T_e above 10eV. Therefore, the profile shape should not influence the inferred S_{ion} strongly. An analysis of the sensitivity has been performed in [45]. 2D inversions of the divertor images were produced from dedicated cameras ('KL11') which view the divertor region tangentially, each camera filtered for a different spectral line including D_α and NII (line radiation from nitrogen ion at 451 nm) [51].

Another measure of the divertor D_α level and extent is through a set of vertically-viewing spectrometer chords shown in figure 2. Each of 5 chords spanning the HT target region provides the brightnesses (C3-C7) integrated through the SOL at the top of the machine and the divertor, the latter being the dominant component due to the low-triangularity configuration used (recycling from the top baffle is negligible). We utilize both the individual chords and the sum of their brightnesses across the divertor, I-D_α.

3. Basic Characterization of shoulder formation

3.1 The shoulder amplitude metric

We define here a simple new metric of the SOL density shoulder amplitude and location based upon normalizing each SOL density profile to its separatrix value. The method, whereby we extract the shoulder peak amplitude and location from the Li beam data, is illustrated in figure 3. The horizontal co-ordinate, $r\text{-}r_{sep}$, is referenced to the mid-plane where r_{sep} is the separatrix radius. We utilize the SOL density profile at a time when the divertor is in sheath-limited (SL) regime (as discussed later, there is an absence of measurable SOL density shoulders in JET in the SL regime) as the reference profile shape (a). This reference profile and all subsequent profiles are all normalized to their separatrix values (b) and their difference to the reference profile is then the measured shoulder profile (c). The maximum of the normalized difference profile is our definition of the shoulder amplitude, A_s, while the location of the peak, r_{As}, is used to follow shoulder expansion towards the limiter (e.g. orange diamonds and black stars in figure 3 b and c). The above method is used for all plasmas studied in this work.

3.2 Dependence of the shoulder on density and plasma current

McCormick, in the first characterization of density shoulders [12], found that SOL density shoulder grew (became flatter) as the line average density, $\overline{n}_e$, was increased (for fixed plasma current, I_p), and the shoulder decreased as I_p was increased. We generally find the same trends with increasing $\overline{n}_e$ for JET density scans (figure 3 (b)). We also find that increasing the plasma current by a factor of two (same increase in toroidal field) at fixed $\overline{n}_e$ (figure 4 (a)) reduces, or suppresses the shoulder as McCormick observed. The near SOL density profile is characterized by an e-folding length of λ_n~ 2cm in all the cases of figures 3 and 4, typical for a wide range of plasmas studied in this paper. We note that as the SOL density profile returns to a single exponential profile, the ion current profile at the target (figure 4 (b)) changes as well – the peak current drops, indicating a less high-recycling divertor. The horizontal co-ordinate, $r\text{–}r_{sep}$, in figure 4 (b), as well as other figures in this paper, has been mapped to the mid-plane for comparison with upstream profiles. Regions where $r\text{-}r_{sep} <0$ are in the private flux region (PFR).

As can be observed from figures 3 (b, c) the location of the shoulder peak moves, or radial extent of the shoulder flattened (large λ_n) region extends outward with increasing core density after the shoulder is fully formed. Such changes strongly increase the density at the limiter radius and thus the ion fluxes to the limiters. Thus, there is first the formation and growth of the shoulder (magenta triangles to green circles to red stars), followed by a shoulder expansion towards the limiter phase (gold diamonds to black pentagons).

4. The correlation of Λ_{div} with shoulder formation and growth

4.1 L-mode plasmas utilizing the outer divertor horizontal target and D_2 fuelling

It is *only* with use of the outer divertor HT in Ohmically heated, D_2 fuelled, L-mode plasmas that enhanced parallel resistivity generally correlates with the flattening of the upstream density profile; other pulse types detailed later in section 4 do not exhibit this correlation. While the data for D_2 fuelled density scans was accumulated from 4 pulses at 4 different plasma currents (with matching variation in toroidal magnetic field to keep the safety factor, q, constant) we will only discuss the 2.5MA case (JPN89346) for clarity. Pulses for all currents from 1.5-3 MA reached detached divertor conditions – defined here as the outer divertor target density, $n_{e,div}$, at the separatrix reached a maximum and then decreased. We use this definition for detachment, as opposed to pressure loss, since a) density is essentially interchangeable with target ion curent (∝ $n_{e,div}T_{e,div}^{1/2}$) whose decrease or 'rollover' is a key measure of detachment; and b) pressure loss is much more difficult to measure accurately. The difference in time between the start of target ion current rollover and pressure loss is, in our experience, small. The core density is increased far past divertor detachment in all cases.

In general, we find that the *shoulder forms, or its amplitude is measureable, just after the divertor plasma transitions from sheath-limited (SL) to high-recycling (HR) conditions.* We define the beginning of the HR regime as the time when the values of density (temperature) and ion current near the separatrix start to increase (decrease) strongly as the core density is increased. One example of the transition to the HR regime is shown in figure 5 where colours and symbols correspond to specific times and $\bar{n}_e$ consistently across all sub-figures as well as the time traces in figure 6. Figure 5(a) displays SOL density profiles from the Li beam mapped to the mid-plane and normalized to the separatrix density (see section 3.1). Uncertainties are not shown but are similar to those shown in figure 4. At low densities (blue squares) SL conditions exist at the outer divertor HT with the peak values of T_e=35eV (d) and n_e=6x10^{18}m^{-3} (b). The corresponding upstream density profile (a) is approximately exponential from separatrix to limiter. The next time point (magenta triangles) corresponds to higher core and divertor densities, the latter rising rapidly under HR conditions and the shoulder begins to form; the peak temperature and density at the target are T_e≈15eV and $n_{e,sep}$=2-3x10^{19} m^{-3}, respectively. As the core density is increased still further, the divertor plasma becomes increasingly high recycling (green circles, red stars) and the shoulder magnitude continues to increase slightly (orange diamonds). At the highest densities (black pentagon symbols) the divertor starts to detach (density at strike point reduces slightly) and, while the shoulder amplitude is not increasing, the shoulder peak location moves radially towards the limiter ($r-r_{sep}$ = 5 cm), raising the density at the limiter radius.

Figure 5 (c) displays the profiles of Λ_{div} at the divertor target plate and how it changes dramatically through the transition from SL to HR regimes with further increases as the divertor becomes more high-recycling. The transition from SL to HR also corresponds to Λ_{div}, rising from below 1 to >10; this increase is more rapid than for the underlying target density and temperature due to the nonlinear dependence of Λ_{div} on those local plasma characteristics (eq. 1; note that $L_{||}$ is calculated as 20% of the connection length from the midplane to the target, a rough measure of the field line length in the divertor). *The correlation between shoulder formation, the transition from SL to HR regimes and Λ_{div} was observed for all HT L-mode $\bar{n}_e$ scans at different values of I_p.*

To emphasize the strong correlation of the transition from divertor SL to HR conditions with shoulder formation, figure 6 displays time traces of the quantities shown in figure 5. Values and error bars shown are moving averages and standard deviations over 100ms respectively – except Λ_{div} where the error is propagated from the underlying n_e and T_e profiles as described. The uncertainties at individual time points are small compared to the error bars shown.

The transition of the divertor from sheath-limited to high-recycling occurs in figure 6 a at ~9.1 - 9.3s, just before the magenta line and triangle markers, as the lower uncertainty of A_s rises above 0. At that time Λ_{div} is in the range of 1-3. After the shoulder appears, A_s increases rapidly to 0.20 while Λ_{div} essentially saturates at values near 50. We note that the saturation of Λ_{div} is at least partially due to T_e saturating at values near 5eV, a common issue for Langmuir probe measurements in tokamaks [52]. $\Lambda_{div,far}$ follows a similar trend to $\Lambda_{div,near}$ (defined in figure 6 caption) but with slightly lower values and larger uncertainties. Gaps in the data are due to strike point sweeping.

The divertor and SOL data from all 4 plasma currents exhibit the same rapid increase in shoulder amplitude, A_s, as $\Lambda_{div,near}$ or $\Lambda_{div,far}$ increase above approximately 1 and divertor (and parallel transport) transitions from SL to HR. The relationship between A_s and Λ_{div} is shown in figure 7 for the two cases of the abscissa being $\Lambda_{div,near}$ (a) and $\Lambda_{div,far}$ (b). The 4 pulses shown span the range of I_p=1.5-3.0 MA for the HT. *Most importantly, the correlation between A_s, and Λ_{div}, appears to be independent of I_p. In addition, we find that a shoulder forms when Λ_{div} exceeds ~1-3 in either the near or far SOL regions.* The appearance of a shoulder above Λ_{div} ~1-3 is similar to the L-mode, *vertical target*, results from ASDEX-Upgrade [32] where the divertor detaches, as opposed to transitioning to HR. The relationship of the shoulder behavior reported in this paper to previous results will be expanded upon in the discussion section.

The expansion of the shoulder peak location, r_{As}, towards the limiter occurs after detachment and with further increases in core plasma density. This is illustrated in the various subfigures in figure 8. During the period when the shoulder forms and grows in amplitude ($\Lambda_{div,near}$ <20-40), r_{As} stays essentially constant for the various plasma currents (figure 8 (a)), 1.8-2.4cm away from the separatrix. At $\Lambda_{div,near}$ >20-40, the divertor plasma is detached and a second phase is entered where r_{As} increases while A_s and Λ_{div} stay ~ constant (Λ_{div} saturates), the expansion towards the limiter phase referred to earlier in the paper. The dependence of r_{As} on core plasma parameters, $\bar{n}_e$ and $\bar{n}_e/n_{gw}$ (figures 8 (b and c)), is more gradual, basically a dependence on $\bar{n}_e$ for a given plasma current; the reason for the dependence on current, or some other related variable, is unclear. The gradual increase in r_{As} with increasing $\bar{n}_e$ also suggests that the drop off in density outside of r_{As} (the second change of scale length) is not due to a limiter or other surface limiting the plasma.

4.2 L-mode plasmas utilizing the outer divertor vertical target and D_2 fuelling

One goal of this study was to determine whether the divertor configuration leads to any changes in divertor conditions and thus in SOL shoulder formation and growth. We know from both modeling and experimental studies that divertor geometry (e.g. VT vs HT) can modify the detachment threshold in upstream density [53-55]. Furthermore, given variations in recycling properties between VT and HTs, there could be differences in the resistivity profile across the divertor target. JET presents an important opportunity to study the effect of the divertor configuration on shoulder formation and characteristics given its fairly unique capability to shift from one configuration to the other with minimal changes in the core plasma.

The L-mode discharges which utilize the VT in our study were operated with the same $\bar{n}_e$ scans through D_2 fuelling and for different plasma currents as for the HT data of the previous section. Time traces for the 1.5 MA VT pulse used in this section are shown in figure 9. As for the HT cases (one at the same I_p shown for comparison), there is a D_2 fuelling ramp (b) that results in a $\bar{n}_e$ ramp (a); more gas must be for VT operation compared to the HT to reach the same $\bar{n}_e$. The strike point ion current (J_{SAT}) (c) rises quickly until ~ 10.5s, after which the density stops rising and then drops (detachment, which occurs at lower $\bar{n}_e$ than for operation with the HT). The corresponding SOL density as well as divertor profiles are displayed in figure 10. The symbols correspond to the same times in both figures. The outer gaps were 5cm, the same as for the HT cases. The values of $\bar{n}_e$ and the separatrix density were similar to those in figure 5 for the HT.

A small but discernable SOL density shoulder appears for operation with the VT. However, this occurs only at the highest $\bar{n}_e$ when the divertor is quite detached. In difference to the HT case, $\Lambda_{div,near}$ and $\Lambda_{div,far}$ have significantly different values; $\Lambda_{div,near}$ *reaches values of order 100 as* the ion current to the target rolls over (not shown) and the peak divertor density decreases (black diamonds), which indicate detachment. In contrast $\Lambda_{div,far}$ is of order 1 to greater than 10 when the shoulder forms; the far SOL region (r-r_{sep}~2.5 cm) does not appear to be detached (no local rollover in target density). Another difference to operation with the HT is that the *divertor* density profile in the far SOL broadens substantially (figure 10(b)).

The different correlation of $\Lambda_{div,near}$ and $\Lambda_{div,far}$ with A_s is shown more clearly for the same pulse in figure 11. Unlike the case for operation with HT operation, A_s does not increase further when $\Lambda_{div,far}$ increases above 10. In summary, for VT operation, $\Lambda_{div,near}$ is a poor predictor of shoulder formation. And even though $\Lambda_{div,far}$ has roughly the same Λ_{div} threshold for shoulder formation as for the HT, the shoulder growth is minimal and general behavior is very different than for the HT.

4.3 Nitrogen seeding to increase parallel resistivity

In the previous 2 sections, we reviewed the results obtained when D_2 fuelling was used to change the divertor conditions while simultaneously changing the upstream conditions ($\bar{n}_e$, $n_{e,sep}$, midplane pressure). To complement those studies, we have utilized a N_2 seeding ramp (figure 12 c) to directly modify the HT divertor conditions while holding upstream conditions such as $\bar{n}_e$ (figure 12 a) roughly constant through constant D_2 fuelling (figure 12 b). The core density reaches an equilibrium value around 9s when the N_2 seeding commences. The effect of the N_2 seeding on the divertor plasma starts around 12s, shortly before detachment start after 13 seconds (~strike point J_{sat} in figure 12 c dropping before 16s).

Moving the divertor condition through HR to detachment by N_2 seeding leads to almost no change to the upstream SOL density profile. This is in stark contrast to the results of section 4.1 (D_2 fuelling only) where there was a strong correlation between A_s and Λ_{div}, calculated for the near or far SOL. Figure 13 displays the usual upstream density and divertor profiles, and corresponding symbols/colors, for the same discharge as Fig. 12. The SOL density profiles (figure 13 a) are not normalized to the separatrix density, unlike previous sections, since the core and separatrix densities hardly vary. The blue squares are the reference profile data from before N_2 injection at 8s, when the divertor plasma is in SL conditions as evidenced by low densities and high temperatures at the divertor target.

A small SOL density shoulder forms (green triangles, 10s in Fig. 12) as $\bar{n}_e$ reaches an equilibrium value; this corresponds to the divertor near SOL being slightly high-recycling. At that point the N_2 injection is initiated, affecting the divertor plasma around 12s which leads the divertor to become even more high-recycling (red circles). Despite this large change in the divertor conditions as well as $\Lambda_{div,near}$ and $\Lambda_{div,far}$, there is very little variation in the SOL density profiles. Finally, at the highest levels of N_2 seeding (gold stars), detachment has begun.

Detachment with N_2 seeding (Λ_{div}~20-40) corresponds to what appears to be *a small reduction of the shoulder amplitude at 16s (Fig. 13a, gold stars) compared to 13s (red circles) as well as a shift in the peak shoulder amplitude outward in major radius* by roughly 1 cm. This is in contrast to strictly D_2 fuelling (Section 3.1, figure 5) where the shoulder amplitude, A_s, is much larger for the same $\Lambda_{div,near}$ or $\Lambda_{div,far}$; *Neither $\Lambda_{div,near}$ nor $\Lambda_{div,far}$ are good predictors of upstream shoulder formation or growth.*

To further demonstrate that increases in N_2 seeding do not lead to increases in the upstream A_s, we utilize Fig. 14a to compare, from the same pulse (JPN90697) as in Figures 12 & 13, periods *prior* to N_2 seeding (up to ~ 12s, blue squares, max. A_s~0.15) to periods *during* the seeding (latter part of pulse, gold triangles, max. A_s~0.10). First, we find that the pre-N injection trajectory of A_s vs $\Lambda_{div,near}$ (blue squares, 'pre-N_2 seed') follows the typical trajectory of unseeded discharges as described in section 4.1 (figure 7). As the N_2 seeding is added (gold triangles, 'during N_2 seeding' later in the same discharge) the data shift to larger $\Lambda_{div,near}$ while the maximum shoulder amplitude, A_s, drops slightly (gold triangles) compared to the data prior to N_2 seeding. In contrast, $\Lambda_{div,far}$ shows almost no change with N_2 seeding other than A_s dropping.

Legacy N adsorbed on vessel surfaces, as reported in [56], can strongly affect the divertor condition and SOL density shoulder in the following pulse. Figure 14 also displays the results (green triangles) from the early part of pulse (JPN90700) before N_2 seeding starts; however, the previous pulse had strong N_2 seeding and thus there is a large amount of N adsorbed on the vessel surfaces. Our only indirect measure of N in the divertor plasma is an NII emission line, the brightness of which is approximately the same for the early part of this pulse (JPN90700) as during the period of HR conditions during N_2 seeding in a previous pulse (JPN90697, same figure).

The 'N loaded' discharge (JPN90700) data follows a trajectory in (A_s vs Λ_{div}) space that is different than pulse JPN90697 and the D_2 fuelled pulses using the HT of section 4.1. In both the near and far SOL, Λ_{div} increases to or above 10 before A_s begins to increase. Figure 14 (a) and (b) thus demonstrate again, similar to the VT vs HT comparison, *that there is no general relationship between* Λ_{div}, with A_s *in either the near or far SOL*; parallel resistivity is not the sole mechanism affecting shoulder growth. We now turn our attention to other mechanisms described in the introduction.

5. Main chamber SOL ionization

In this section, we present evidence that suggests local ionization in the main chamber SOL does not strongly influence the shoulder formation. Figure 15 displays a comparison of two (D_2 fuelled) density ramp pulses, one each utilizing the HT and VT configurations, plotted with solid and dash-dot lines, respectively. Normalized density profiles (a), and ionization rate profiles (b), are shown for the three $\bar{n}_e$ selected at the times corresponding to the vertical lines in (c), which displays the midplane neutral pressure (Penning gauges). Separatrix densities were also equal for each divertor target configuration and $\bar{n}_e$.

Despite the lack of shoulder, the local neutral ionization rate, S_{ion}, is of slightly greater magnitude for VT operation for all $\bar{n}_e$; this may be due to higher divertor D_2 fuelling rates being required for the vertical target vs horizontal target operation to achieve the same $\bar{n}_e$. Further, the shape of the S_{ion} profile in the HT is broader when a shoulder is present. *This indicates that the shape of the ionisation profile is more determined by the* n_e *profile, rather than vice versa.*

Additionally, the mid-plane pressure, measured by Penning gauges, shows an equivalent functional dependence on $\bar{n}_e$ for both target configurations (figure 15 (c)). This indicates that the magnitude of the influx of neutrals toward the plasma cannot be solely responsible for setting the profile shape, consistent with the ionization profile shown in (b); the broadened S_{ion} profiles for the HT are due to the increased density in the far SOL rather than an increased influx of neutrals.

These results indicate that ionisation of midplane neutrals (shoulder formation mechanism c) is not sufficient, or possibly even necessary, to flatten the density profile and that there must be some other mechanism which influences the shoulder formation.

Given that separatrix densities & temperatures and core conditions were equivalent for each divertor target configuration and $\overline{n}_e$, potential shoulder mechanism a) is also unlikely to be a determining factor in shoulder formation unless SOL radial transport is affected by the change in divertor configuration; For example, later in this paper we show that changes in divertor recycling accompany changes in divertor configuration. Changes in the divertor recycling pattern could lead to changes in radial electric field which has been postulated to change turbulent filament birthrates[57].

6. Divertor neutral processes

Divertor neutral processes could be reducing the loss of ions out of the upstream SOL – the so-called ion 'sink' or drainage mechanism for upstream shoulder formation (shoulder formation mechanism d), outlined in the Introduction. Our primary measure of neutral processes in the divertor is through the intensity and distribution of D_α, which can be roughly related to the distribution of both ionization and charge exchange (CX). The connection between those processes and parallel flows will be discussed in more detail in the Discussion section.

The ionization rate, $S_{ion} = n_e n_0 <\sigma v>_{ioniz}$ is dependent on n_0, the neutral density, and $<\sigma v>_{ioniz,}$ the electron ionization rate coefficient. S_{ion} has a similar functional dependence on temperature as the D_α emission rate for temperatures of 10eV and above (dominated by excitation in attached plasmas). The result is that the number of ionizations per emitted D_α photon does not vary much in this range (but does not take into account ionizations occurring through molecules; we estimate this to be roughly a factor of 2 effect). Therefore the magnitude of divertor D_α is a good proxy, in a relative sense, for the amount of divertor ionization in this temperature range. Between 10 eV and 5 eV, or potentially lower, the number of ionizations per D_α photon drops by a factor of ~ 2.

The divertor D_α emission region is also a good proxy for the extent as well as the number of CX reactions occurring in the divertor ($S_{CX} = n_i n_0 <\sigma v>_{CX}$). Both the charge exchange and D_α excitation rates are, again, fairly constant above 10 eV. For T_e below 10eV, the number of charge exchange events per D_α photon increases since the D_α excitation rate is dropping.

As described in Section 2, we monitor the divertor D_α by both chordal spectroscopy measurements of D_α through the divertor cross-section, as well as toroidally-viewing camera images of the divertor region, filtered for D_α, which are tomographically inverted to provide a 2D pattern of D_α

emissivity (photons/(m^3s)).

6.1 Strike point sweeping and effect on upstream density shoulders

Through minimal radial sweeping of the strike point across the HT (total target distance of 5 cm) we find that the changes in the total D_α emission across the divertor (I-D_α, the sum of chordal D_α brightnesses C3-C7 passing through the outer divertor plasma) oscillates in the same sawtooth fashion as the strike point location, $R_{strikepoint}$ (figure 16 (a)). The close correlation between movement of the strike point, A_s, and I-D_α, is shown in figure 16 versus time. Note that the pulse shown is the same as in Figures 12 and 13. However, Fig. 16 only displays the sweeping period over which the core density is constant, so constant high recycling conditions, and before the N_2-seeding has an effect on the divertor plasma.

Following the formation of a small shoulder (figure 16 b, 8.5s), the strike point sweeping starts and both A_s (16 b) and I-D_α (16 c) oscillate in anti-phase with respect to the radius of the outer strike point, R_{sp} (figure 16 c). In other words, I-D_α (and A_s) are both maximized when R_{sp} is smallest - when the strike point is farthest from the entrance to the pump and thus fewer neutrals are being removed.

Figure 17 displays the correlation between the upstream shoulder amplitude and divertor characteristics given in figure 16. The strong correlation between A_s and I-D_α (b) as well as between I-D_α and R_{sp} (a) quantitatively reflect what is evident from figure 16; small changes in the divertor D_α (and thus ionization and charge exchange) correlate with observable changes in A_s upstream. The working midplane limiter probe J_{SAT} (not shown) oscillates in phase with A_s (and I-D_α), thus consistent with a shoulder increasing and decreasing.

In contrast to I-D_α, Λ_{div}, within error bars, does not change with A_s (figure 17 c and d). There is also little effect on target peak J_{SAT} during the sweeping period (see Fig. 12). That is consistent with little to no change in divertor profiles (n_e, T_e) during the sweep (not shown) and could indicate that the large variation in I-D_α is due to the divertor leg sweeping through a radial gradient in neutral density (lowest neutral density nearer to the pump).

We have also investigated the cross-correlation time delay between A_s and R_{sp} as well as A_s and I-$D_{\alpha.}$ The cross-correlation time for the latter two variables is ~0 within the time resolution of A_s (10 ms). This is consistent with changes in the divertor I-D_α, representative of neutral processes, directly leading to changes in the upstream density profile. We will discuss that connection more in the discussion section.

In summary, strike point sweeping during periods of constant fuelling and core density leads to a modulation of the shoulder amplitude, while the upstream separatrix and divertor densities and Λ_{div} do not measurably change; there is a case where A_s *varies without any change in* Λ_{div}. The implication is that there is some divertor-derived mechanism other than parallel resistivity affecting upstream shoulder formation/growth. That mechanism, explored in the next section, could be related to divertor neutral processes as quantified by I-D_α.

6.2 Comparison of vertical vs horizontal target divertor D_α emissivity profiles

Another test of whether divertor D_α, and thus divertor neutral processes, are affecting upstream density shoulder profiles is to explore that connection for changes in divertor geometry through examination of figure 18. Contour plots of D_α emissivities derived from KL11 D_α camera image (section 2) inversions are displayed given the vertical chordal measurements used in I-D_α do not properly cover the vertical target.

Examining the first column (figure 18 a and d) where the divertor plasma is in the SL regime: we find that there are only slight differences in the D_α magnitude and extent between HT and VT configurations. The slight shift of the VT D_α emissivity region into the private flux region is within uncertainties in EFIT as well as the unknown amount of reflections. However, the shift could also be due to the divertor geometry; recycled neutrals from a HT would mostly travel towards the common flux region while, for the VT, recycled neutrals move towards the private flux region. Such directional differences in recycled neutrals would be consistent with higher measured sub-divertor pressures for the VT compared to the HT for a given $\bar{n}_e$.

The difference in D_α emissivity profiles between HT and VT operation becomes pronounced as the shoulder is formed. Figure 18 (b and e) correspond to a later phase in the same pulse where both configurations have transitioned to HR divertor conditions. The upstream SOL density shoulder has formed for the HT configuration, but not in the VT configuration. Firstly, the HT peak emissivity is ~ 2x higher than for the VT. Secondly, there is a clear difference in the shape of the emission region; the equivalent contour line (e.g. red) for the HT configuration extends over a wider region (x2) towards the common flux region of SOL, than for the VT.

As the core density is increased further (figure 18 c and f), the shoulder amplitude approaches saturation for the HT case, which is still in a high-recycling condition. The region of high D_α emissivity for the HT configuration has continued to spread across and along flux surfaces and possibly to larger R, spreading over the edge of the HT (R>2.82m) if the inversion is to be trusted.

In contrast, the D_α emission region area and maximum D_α emissivity remain relatively unchanged for the VT case.

Thus, as the divertor becomes more high recycling and an upstream shoulder forms for the HT case but not for the VT, the area and total outer divertor D_α *emission are smaller for the VT case.*

6.3 The effect of N_2 seeding on divertor D_α profiles and magnitude.

It was shown in section 4.3 that N_2 seeding causes Λ_{div} to rise strongly without a corresponding increase in the upstream SOL density shoulder. In contrast to D_2 fuelling, N_2 seeding acts to reduce the divertor D_α emission, consistent with the lack of increase, or possible decrease in upstream density shoulder amplitude.

This behavior is demonstrated in Figure 19, which shows signal traces from a later phase in the pulse discussed in section 6.1 (JPN90697) where N_2 seeding is used. The divertor NII brightness (a), which is a rough measure of the N level in the divertor, increases concurrent with the reduction in A_s (Fig. 19b, strike point sweep is causing A_s to oscillate). Traces C3-C7 show vertically viewing chordal measurements through the HT region (see figure 2 for chord locations) of D_α brightness from x-point major radius (C3 view) to R slightly greater than $R_{strikepoint}$ (C7 view). At low levels of NII brightness, the oscillation in D_α is visible on all channels. Increasing levels of N in the divertor correspond to drops in the D_α brightness of chords C5-C7 as well as brightness oscillation. The decreases in brightness occur initially for the largest R channels (C6 and C7), moving progressively inwards in major radius to C4. We think the changing brightness profiles correspond to movement of the peak D_α brightness along the separatrix towards the x-point given the contour plots like those in Fig. 18 and shown previously in a recent paper by Field[58]. As the overall D_α emission region shrinks, A_s decreases; even if the divertor T_e is constant during the seeding ramp the amount of ionization and charge exchange events is likely decreasing – even more reductions should occur if the divertor T_e is dropping. The sub-divertor neutral pressure (not shown) remains constant over this time range.

Unlike $\Lambda_{div,}$ I-D_α is well-correlated with shoulder formation regardless of whether N is present in the discharge or not. Positive correlation is observed between A_s and I-D_α as shown in figures 16 and 17 where Λ_{div} was essentially not varied. This behavior is again demonstrated in Figure 20: The data from JPN90697 (blue squares) includes a step up of the D_2 fuelling (Fig. 16) to a constant value for the remainder of the pulse in order to achieve a small shoulder followed by the start of a radial sweep of the strike point. The corresponding increase of A_s and I-D_α during the density increase clearly overlaps with the trajectory of a standard density ramp of section 4.1 (JPN89346 black circles). Once the sweep starts, there is deviation from the case of only D_2 fuelling, consistent with only varying I-D_α as opposed to Λ_{div} (see section 6.1). Note that core density and Λ_{div} are held constant during the sweep as shown in Figure 16 and 17.

The third discharge included in figure 20 includes another layer of difference – namely the level of N still in the machine from previous pulses, 'N-loading'. This discharge (green triangles JPN90700) was previously used (figure 14) to demonstrate how Λ_{div} was a poor measure of shoulder amplitude, A_s. Here, we first find during the density ramp that I-D_α follows the trajectory of the unseeded HT cases (black circles, blue squares) unlike for the case with Λ_{div}, shown in Fig. 14. This similarity between the N-loaded (green triangles) and pure D_2 fuelled (blue squares) cases continues during the period of strike point sweepings; I-D_α and A_s respond in the same way to strike point sweeping for either case – with or without N-loaded surfaces; N-loading suppresses both the I-D_α and A_s variation.

In all the cases shown in figure 20, with N_2 seeding or without, with sweeping or without, I-D_α, unlike Λ_{div}, correlates well with A_s.

7. Shoulder formation behavior in H-mode

While the research focus of the previous sections of this paper focus on L-mode plasmas, we have studied a few H-mode discharges where the ELM frequency was low enough to make measurements between ELMs. ELMs are major perturbations on the SOL and divertor plasma, where plasma characteristics are strongly varying within the measurement time resolution. The H-mode plasmas we show correspond to the outer strike point on the HT. Ramps in fuelling and nitrogen seeding were available and thus are easily compared to the equivalent L-mode discharges. In general, the behavior of SOL density shoulders in H-mode plasmas was similar to that of a comparable L-mode discharge.

7.1 H-mode D_2 fuelling ramp

The first case we address is the simplest of the previous sections, in which shoulders are also most evident – a D_2 fuelling ramp, which moves the divertor condition from sheath-limited through high-recycling. Figure 21 displays the time dependence of several core and divertor plasma parameters. Despite the factor of 8 increase in D_2 fuelling rate, there was little change to $\bar{n}_e$, although Γ_{div} (integral of ion current over the outer divertor) increased somewhat. The D_2 gas was injected through GIMs 10 (SOL or common flux region, see Figure 1 & 2) and 11 (private flux region), different from the L-mode cases in the sense that GIM 10 is used instead of GIM 9, which was also in the SOL. In the course of the fueling ramp, the ELM frequency increased from 25 to 100Hz. Vertical shaded bars with corresponding symbols indicate periods where the divertor and SOL data has been analyzed; the width of the shaded regions corresponds to the length of time over which data is averaged in the following description.

ELMs increase the density in the SOL rather than change the time-averaged profile shape. The SOL density profile 'between ELMs', shown in figure 22, is created by averaging profiles obtained during multiple inter-ELM periods during the shaded period (yellow) around 52.5s in figure 21. The profile labeled 'including ELMs' is averaged over multiple Li-beam measurement periods, but for frames including ELMs. The relatively weak increase in the normalized density of profiles which include ELMs is due to the exposure time of the Li beam being 2-3 times longer than the duration of the ELM.

The evolution of the divertor profiles of n_e, T_e and Λ_{div} during an H-mode fuelling scan shows little difference to L-mode HT plasmas. The profiles with different symbols/colors shown in figure 23 correspond to the color shaded regions of figure 21 (inter-ELM periods). In the L-mode phase (blue squares) the divertor n_e (b) and T_e (d) profiles indicate slightly high-recycling conditions and a small upstream density shoulder. Upon transitioning to H-mode (green triangles), the density profile in both the near and the far SOL becomes steeper, consistent with the H-mode reduction in radial particle and energy transport. Simultaneously, the divertor transitions from HR to SL conditions as the divertor target n_e reduces, and T_e increases strongly (leading to Λ_{div} decreasing); the small shoulder disappears. Thus the L-mode relationship between the upstream density profiles and target conditions holds across the L-H mode transition for the case of HT D_2 fuelling ramp).

With increasing gas fueling, the divertor becomes more high recycling (red circles to black diamonds) and the corresponding Λ_{div} increases. Similar to the L-mode discharges of section 4.1, a density shoulder forms in the upstream SOL. With further increases in the D_2 fueling rate, the shoulder amplitude and the density at the limiter radius substantially increase, correlating with broadening of the divertor density profile as shown previous for the VT case (Fig. 10). It may be that the inner edge of the shoulder moves towards the separatrix (broadening) which could mean that the near SOL region contracts (red circles to black diamonds). Detachment did not occur, even for the latest time point.

7.2 **H-mode N_2 seeding ramp**

As for the L-mode case (sections 4.3 & 6.3), divertor N_2 seeding does not lead to further flattening of the upstream density profile. Figure 24 displays time traces for an N_2 seeding ramp (Fig. 24c) where D_2 fuelling was held constant (Fig. 24b). We note that the ELM frequency was substantially lower than for the D_2 fuelling ramp case of figure 21, as has been previously observed [59].

The density profiles (Figure 25a) at the lowest Λ_{div} already show substantial flattening and since the 'reference' profile is not exponential, any inferred value of A_s (Figure 25c) cannot be directly compared to the L-mode cases. We do not determine a shoulder amplitude given the absence of a reference single-exponential SOL density profile.

During the transition to H-mode (green triangles) the near SOL density profile steepens as observed for the D_2 fuelled case (Section 7.1). The divertor conditions are sheath-limited, indicated by high T_e (see Fig. 25c). As $\overline{n}_e$ increases later into the H-mode (red circles), the density profile in the far SOL is essentially the same as the L-mode.

The subsequent rise in N_2 seeding does not modify the upstream density profile outside of uncertainties, yet there are strong changes to the divertor conditions and also Λ_{div}. First the target density rises (black stars) followed by the plasma detaching as indicated by the drop in peak density (maroon diamonds, cyan pentagons) in Fig. 25b and the ion target current (Γ_{div} in Fig. 24e). In the most detached case, $\overline{n}_e$ and $n_{e,sep}$, are slightly higher and yet there is no appreciable change in the far SOL density. In fact the far SOL density would be dropping if all the profiles were normalized to the separatrix values as done for earlier cases shown.

As shown in figure 25 (c), Λ_{div} reaches a maximum just prior to the onset of detachment which occurs after the density peaks (black stars) and when the divertor target ion current rolls over (~ 10-11s, Fig. 24e). The collisionality will continue to increase as detachment occurs. From this it follows that the dynamic range of Λ_{div}, when using target Langmuir probes, does not extend into detached conditions. Thus, *strong increases in Λ_{div}, beyond what is measureable, are occurring and do not necessarily lead to further flattening of the density profile and thus enhanced main chamber radial fluxes, whether in L-mode or H-mode.*

8. Discussion

The purpose of this study was to investigate possible mechanisms that control SOL density shoulder formation. As discussed in the introduction these include, in general terms, SOL radial transport, SOL particle sources or sinks (parallel transport) for ions. Here we review and discuss the various mechanisms studied in this paper.

8.1 The role of upstream conditions in shoulder formation

The results contained herein indicate that varying the divertor configuration brings a new tool to investigating the physics leading to SOL density shoulders. Under the same separatrix conditions and midplane neutral densities, SOL density shoulders appear when the outer strike point was on the horizontal target (HT) but not for vertical target (VT) operation (section 5, particularly Fig. 15). Such results indicate that it is unlikely that separatrix conditions (n_e, T_e, gradients, ….) are directly influencing SOL radial transport (shoulder formation mechanism a), or that fuelling of the upstream SOL is locally increasing the local density (shoulder mechanism c); neither appear to be mechanisms directly contributing to shoulder formation and growth.

We note that there is no clear agreement across the tokamak research community as to whether SOL ionization is raising the density in the SOL. An experimental study of shoulder formation on MAST [17] also found no correlation between a radial D_α chordal measurement at the plasma mid-plane, associated with ionization, and changes to the profile flatness. The authors of [60] pointed out that if there was enough local ionization to affect the density profile then the local T_e should drop as the ionization energy is an energy loss and new ions (coming from cold neutrals) will have lower plasma temperatures – this is not observed in that study or at C-Mod [61]. In addition, modelling of the SOL concluded that local ionization is likely not a strong effect [62].

Lipschultz initially pointed out [13] that when the mean free path for ionization of neutrals and charge exchange, $\lambda_{iz,cx}$, is small, on the order of the thickness of the SOL – a so-called radial high recycling condition could follow; ionization raises the local density leading to more ionization and further density rise. This logic has recently been advocated as well [34, 35] as a second mechanism, working in tandem with parallel resistivity, to create shoulders. While the SOL ionization characteristics described above for JET don't seem to support that second mechanism, one would expect that increased SOL densities due to shoulder formation will always lead to more ionization in the SOL, but this is not necessarily evidence of a positive feedback loop and the existence of the radial high-recycling condition; parallel losses would increase as well if the local Mach number stayed constant. At least for JET (Fig. 15), it appears that increased SOL ionization as the SOL density shoulder grows is a symptom of shoulder growth as opposed to being a cause.

A second difference of the JET SOL ionization measurement to that in ASDEX-Upgrade is that the JET D^0 ionization profile is peaked near the separatrix (Fig. 15) as opposed to the limiter radius (modeled, not measured, for ASDEX-Upgrade [34, 35]). Similar separatrix-peaked ionization profiles have been measured for C-Mod and DIII-D [13] as well as a previous study of JET [63].

We have noted that after the SOL density shoulder completely forms, a second phase follows, correlating with detachment for the HT; the shoulder extends/expands towards the limiter. Ionization could be contributing to this expansion of the shoulder to larger R, but we cannot comment on that contribution relative to other mechanisms such as changes in parallel losses.

What is clear is that it would be useful to produce more detailed studies of the profile of the ionization source rate across the SOL, its correlation with shoulder formation/expansion and comparison to estimates of parallel losses and changes in turbulent transport along and across the magnetic field.

8.2 Parallel resistivity

There is broad agreement between our study and those on TCV [33] for L-mode discharges where increases in parallel resistivity ($\Lambda_{div} > 1$) are a 'necessary', but *not* a 'sufficient' condition for SOL density formation. This conclusion came from a set of discharges where $\Lambda_{div} >> 1$ (near or far SOL) and yet, in some cases SOL density shoulders occurred, and in other discharges shoulders did not form [33]. In the case of our JET L-mode studies we reach the same conclusion but through different tests: In the case of N_2 seeding, changes in Λ_{div} do not lead to increases in shoulder amplitude, with indications that shoulder amplitude can decrease. In the case of strike point sweeping (Fig. 17) shoulder amplitude varies without any change in Λ_{div}, only correlating with changes in divertor Balmer alpha emission, I-D_α. In contrast to the JET results use of N_2 seeding in ASDEX-Upgrade L-mode discharges [16,17,34] does lead to shoulder amplitude increase - 'These results are independent on how *detachment* is achieved').

The more recent ASDEX-Upgrade study [34, 35] of H-mode discharges also point towards increases in parallel resistivity not being sufficient to lead to shoulder increases; N_2 seeding still leads to shoulder formation, but *only if accompanied with 'high' D_2 fuelling*. The single H-mode JET discharge with N_2 seeding included in our study does not evidence any increase in shoulder with increasing Λ_{div} through N_2 seeding, However, the constant JET D_2 fuelling might be considered 'low' D_2 fuelling.

The question of what other mechanism besides parallel resistivity is required for shoulders to form is addressed again in section 8.5.

8.3 Divertor neutral processes

The insufficiency of increases in parallel resistivity (Λ_{div}), in correlating to changes in SOL shoulder properties in all cases led us to the search for whether there was an alternative mechanism/measurement that correlated better with shoulder formation and growth. Based on the results presented in section 6, we speculate that increases in 'recycling' or 'neutral processes' in the divertor, as quantified by I-D_α, are leading to shoulder formation/growth.

The divertor D_α emissivity, summed over the outer divertor region, I-D_α, correlates well to upstream density shoulder amplitude: a) It does rise with D_2 fuelling in correlation with A_s for the HT as does Λ_{div}; b) *It does not rise* (nor does A_s) as N_2 seeding is used to make the divertor more recycling and increase Λ_{div}; c) Sweeping of the outer strike point back and forth across the HT strongly varies I-D_α in direct correlation with upstream shoulder amplitude variations (and essentially immediately, within the time resolution of the diagnostic) *without* changes in Λ_{div}; and d) switching from HT (shoulder) to VT (small, or no shoulder) geometry lowers I-D_α and A_s and shrinks the region of high D_α emission away from the far SOL, the location of the upstream density shoulder.

All of the above correlations of I-D_α with A_s indicate that I-D_α is a more consistent indicator of shoulder changes than Λ_{div}. But a more detailed study is needed, along with modeling, to better understand the roles of underlying processes.

The strike point sweep data could be seen as complementary to the switch between horizontal and vertical targets: When the strike point on the HT is closest to the vertical target the amount of divertor D_α is lowest (as well as A_s); when the strike point is farther from the vertical target the amount of fivertor D_α is highest as is A_s. The reduction in divertor recycling may be lowest when the strike point is at the entrance to the pump at ~ 2.9m where one assumes that the neutral density will be lowest.

EDGE2D-EIRENE modelling of unseeded H-mode plasmas utilizing the vertical and horizontal outer targets [64] shows similarities to the experimental results presented here. The modeled divertor ionization distribution at the target is much broader in HT compared to the VT configuration. The density across the entire SOL was increased for HT compared to VT, although the profile shape was generally the same. The lack of a localized effect in the region of the upstream density shoulder may not be surprising given such fluid codes do not take into account cross-field transport due to turbulence or even convection.

There is a significant literature base that supports the connection between increased divertor ionization leading to lower flows into the divertor – a mechanism that can reduce the loss of ions, or their ‘drainage’ from the upstream SOL and thus increase the upstream density (shoulder formation mechanism d). Ionization in the divertor plasma has been shown in multiple models (fluid and analytic) to affect flow magnitude and direction, even leading to ‘reverse flows’ out of the divertor towards the SOL[65-69]. Variations in flows can be localized and thus could affect just to regions of the divertor which could correspond to the upstream SOL shoulder region. In addition, we also know that charge exchange processes can directly lead to reduced flows in the divertor as well through momentum removal (particularly detachment). The authors of [60] even argued, independent of detachment, that 'the CX induced friction with the neutrals over the entire flux tube slows down the plasma motion towards the target hence "clogging" its flow out of the SOL'.

A recent model by Walkden [42] relating SOL filament characteristics to SOL shoulders also pointed towards reduced parallel flows out of the SOL as an important mechanism for SOL density shoulder formation. The model compares parallel resistivity, upstream ionization and drainage as mechanisms for shoulder formation based on a stochastic framework for turbulence characteristics. Increased ionization, as a source for ions, cannot be differentiated in that model from a decrease in ion drainage so they should be viewed as the same for that study. Walkden found that local reductions in parallel losses to the divertor (or SOL ionization) could match JET shoulder formation and growth [42]. On the other hand he found that increases in Λ_{div} across the SOL did not lead to shoulder formation, only to expansion of the shoulder extent once formed. Walkden points out that the study was not exhaustive and did not constitute a definitive rejection of parallel resistivity and turbulence characteristics leading to shoulder formation and growth.

There are also direct measurements of parallel flow in the upstream SOL that do not support the reduction of flows with increasing density. Lipschultz's summarization of measurements of the parallel flow velocity profile over several tokamaks [13], indicate that parallel flows toward the divertor *increase* with increasing density in the near SOL of JET and C-Mod; those measurements do not take into account ExB flows. Hidalgo et al's measurements of SOL turbulence characteristics on JET [70] led to the statement that 'as the size of transport events increases, parallel flows also increase'; this would indicate that as parallel resistivity increased, and thus increases in filament size, parallel ion losses would *increase* instead of *decrease* as required to increase the SOL density.

There are suggestions in the literature of another mechanism that could change upstream cross-field transport and be related to changes in divertor configuration and recycling. Modelling of the effect of differences between horizontal and vertical-target JET divertor configurations shows differences in radial electric fields in the divertor and upstream SOL [71]. This is shown to be due to differences in recycling in the divertor leading to differences in the T_e profile across the divertor; the T_e profile is more peaked at the strike point for the HT vs VT cases (One can see an example of this in comparing our Figures 5 and 10). Chankin suggests that the enhanced E_r leads to turbulence shearing and easier access to H-mode[71]. Fuchert, although not addressing divertor effects, argues that the magnitude of E_r (in the region of the separatrix) may play an important role in determining the filament birth rate and hence transport[57]. Such ideas may explain the difference between HT and VT achievement of SOL density shoulders but might not for the case of strike point sweeping effects on the upstream density shoulder.

In summary, we have no direct proof that divertor neutral processes are leading to shoulder formation through either reductions in parallel flows out of the upstream SOL or changes in electric fields. However, the changes in I-D_α are well-correlated with changes in the SOL density shoulder over a wide range of conditions where $\Lambda_{\rm div}$ is not. This motivates more investigation of the relation between plasma-neutral processes in the divertor, electric fields and main chamber radial transport whether inside or outside the separatrix.

8.4 Shoulders and H-mode plasmas

Evidence of density shoulders in the SOL of H-mode plasmas is relatively sparse in the literature. To the best of our knowledge, this paper presents the first measurements of shoulders in H-mode plasmas for the JET-ILW. N_2 seeding utilizing the horizontal target for the outer divertor led to even higher values of collisionality than L-mode, and yet changes to the SOL density profile were *still* not observed. This adds to the strong evidence against $\Lambda_{\rm div}$ as a sufficient control parameter.

8.5 Implications of this work

What leads to the situation where Λ_{div} rises strongly and no shoulder increase occurs? Is this consistent with Λ_{div} being a necessary condition [33, 35] for shoulder formation and/or growth? Λ_{div} can only be a necessary condition for shoulder growth or formation if, as Carralero states [35], there is a second mechanism (midplane ionization close to the limiter radius) that, combined with Λ_{div} above a threshold value, leads to shoulder formation and growth. Our results are not consistent with near-limiter ionization as the second mechanism, primarily because of the results of sections 5 and 8.1; *our results indicate that any second mechanism would need to be related to divertor neutral recycling as quantified by I-D_α.* It is certainly true that I-D_α increases along with Λ_{div} during density scans but I-D_α (or A_s) does not increase along with Λ_{div} with N_2 seeding. In addition, variations in I-D_α obtained through strike point sweeping are consistent with variations in shoulder amplitude even when there is no variation in Λ_{div} (we note that Λ_{div} is above 1 in those cases).

While our JET results are consistent with Λ_{div} being a necessary condition for shoulder formation and growth (Λ_{div} is always above 1 when shoulders are observed), *one should also consider the possibility that while changes in parallel resistivity do lead to changes in filament nature, those changes are not leading to changes in the SOL shoulder profile*; this is also suggested by the Vianello results[33].

Could changes in Λ_{div} be merely coincident in some parts of operating space with a different mechanism for shoulder formation/growth? We, and others have pointed out that a reduction in parallel losses along the magnetic field from the SOL shoulder region to the divertor could lead to an increase in density in the SOL. This would be consistent with initial modelling of JET density shoulders based on the statistical nature of filaments discussed above [42]. A second shoulder formation mechanism consistent with changes in divertor recycling would be through changes in divertor and SOL E_r [57, 71]. More modeling of such effects could help guide experiments.

It is also worth noting that shoulder formation and growth are robust features of reduced edge turbulence codes such as ESEL [14, 72] although the parallel resistivity is not explicitly included within these models. Simulations of this kind are advantageous since they self consistently generate filaments, which a statistical approach cannot.

We should also take this opportunity to point out that, at least for JET, there is a difference between shoulder 'formation' and 'growth'. In the case of C-Mod [61] and ASDEX-Upgrade (e.g. [15, 16, 34]) the SOL profiles shown always display a near and far SOL which, by the definition given (see Introduction), means that the SOL cannot be characterized by a single exponential falloff length. In that sense shoulders have already formed in those tokamaks and, in the case of ASDEX-Upgrade, the far SOL falloff length is found to suddenly increase once Λ_{div} increases past a threshold of 1 and other conditions are met. For JET the situation is somewhat different – shoulders form (the appearance of a far SOL) when Λ_{div} and I-D_α both increase through changes in divertor recycling, and then grow. There are also differences in formation and growth for the vertical- vs horizontal-target in JET. The cause(s) of the above differences are not clear and we refrain from speculating. But we recommend that future work addresses shoulder formation as well as growth where possible.

Based on the existing database of shoulder studies it seems unclear what we can predict for ITER; in our opinion there is no quantitative model and agreed upon shoulder formation/growth mechanism(s) that is consistent with measurements that leads to shoulder formation. Certainly the ITER divertor will be in a high recycling and even partially detached condition and N_2 seeding is likely (but this has no effect on the shoulder). However, under such conditions with L-mode plasmas and a vertical target, the shoulders are very small on JET while larger on C-Mod and ASDEX-Upgrade. We do not know how to reconcile this difference at the moment. Another problem with extrapolating to ITER is that the database of shoulder studies for H-mode plasmas is small compared to that for L-mode plasmas making extrapolation even more risky. Lastly, the database of SOL density shoulder physics is limited to gas-fuelled plasmas which have SOLs that are much less opaque to neutrals than ITER [5]; ITER will thus rely on pellet fuelling. In the end models that predict current results are required for any predictions of ITER SOL characteristics and first wall interaction.

9.0 Summary

The research presented herein complements previous studies of SOL density shoulders which centered on SOL turbulence. Herein our focus is primarily on the role of the divertor in shoulder formation through: 1) in-depth measurements and analysis of the divertor profiles; 2) the study of the potential role in shoulder formation of both the divertor and midplane recycling; and 3) important information about the effect of divertor configuration which completely changes the character of shoulder formation, growth and expansion, likely through changes in divertor recycling.

We have explored four mechanisms, outlined in the introduction, which could affect the formation and growth of density shoulders in the far SOL.

We find that the probability of upstream mechanisms (core/separatrix density and temperature changing radial transport or a local ionization source) being responsible for shoulder formation is low. SOL density shoulders form and expand for the case of discharges with outer strike point on the horizontal target while, for the same core/separatrix density and temperature (assuming filament birth characteristics held constant) and midplane neutral pressure (neutral influx and total ionization held constant), shoulders do not form when the vertical target is used. *If upstream SOL density shoulder mechanisms were important then divertor configuration should not matter.*

Turning to the effect of increasing parallel resistivity, Λ_{div}, on the upstream SOL density profile our conclusions are similar to those reached by Vianello [33] and Carralero [34]: namely that increases in Λ_{div} *are not sufficient* to lead to shoulder formation. And IF $\Lambda_{div} > 1$ is necessary for shoulders to form, a second mechanism is necessary as well. *Our results point towards divertor recycling (quantified by I-D_a) as that second mechanism or, potentially, even the primary mechanism for shoulder formation.*

Our results do imply that changes in ion-neutral processes in the divertor, as measured through the distribution and magnitude of D_a (I-D_a), are more consistent with shoulder formation/growth than parallel resistivity. In contrast to $\boldsymbol{\Lambda}_{div}$, I-$D_a$ *does* increase with upstream shoulder amplitude under D_2 fuelling and *does not* increase with N_2 seeding (no shoulder increase). I-D_a is smaller for outer divertor vertical target discharges where shoulders are small and difficult to form. Finally, strike point sweeping showed that upstream shoulder amplitude varies with I-D_α; this is without changes in $\boldsymbol{\Lambda}_{div}$. Using existing literature we show that the connection of I-D_α to upstream SOL shoulders could be through such underlying physics processes as changes in parallel losses from the SOL or radial electric fields, which can affect turbulence and poloidal flows.

When the horizontal target divertor is pushed into detachment with D_2 fuelling the upstream density shoulder amplitude stops increasing and there is an expansion of the shoulder region towards the limiter radius. Such behavior may be due to local SOL ionization as the mean free path for ionization of neutrals in the SOL (launched from limiters or wall surfaces) shortens and the neutral influx increases.

We have briefly examined the SOL and divertor characteristics during the period between ELMs for H-mode discharges. Although only two discharges were examined, the same differences between shoulder formation with D_2 fuelling and N_2 seeding found for L-mode plasmas transfer to H-mode.

10. Acknowledgements

The authors are grateful for discussions with N. Vianello and D. Carralero as this study progressed. This work has been carried out within the framework of the EUROfusion Consortium and has received funding from the Euratom research and training programme 2014-2018 under grant agreement No 633053. The views and opinions expressed herein do not necessarily reflect those of the European Commission. We also acknowledge support from the EPSRC grants EP/L01663X/1 and EP/K504178/1, which fund the University of York, EPSRC-funded, Centre for Doctoral Training in the Science and Technology of Fusion Energy. The research by B. Lipschultz was funded in part by the Wolfson Foundation and UK Royal Society through a Royal Society Wolfson Research Merit Award as well as by the RCUK Energy Programme (EPSRC grant number EP/I501045).

References

[1] Pitts, R, Kukushkin, A, Loarte, A, Martin, A, Merola, M, Kessel, C, Komarov, V, et al., "Status and physics basis of the ITER divertor", Physica Scripta, **2009** (2009) 014001.

[2] Eich, T, Leonard, AW, Pitts, RA, Fundamenski, W, Goldston, RJ, Gray, TK, Herrmann, A, et al., "Scaling of the tokamak near the scrape-off layer H-mode power width and implications for ITER", Nuclear Fusion, **53** (2013) 093031.

[3] Stangeby, PC, The Plasma Boundary of Magnetic Fusion Devices, Institute of Physics Publishing Bristol, 2000.

[4] Pitcher, CS, Stangeby, P, "Experimental divertor physics", Plasma Physics and Controlled Fusion, **39** (1997) 779.
[5] Lipschultz, B, Bonnin, X, Counsell, G, Kallenbach, A, Kukushkin, A, Krieger, K, Leonard, A, et al., "Plasma-surface interaction, scrape-off layer and divertor physics: implications for ITER", Nuclear Fusion, **47** (2007) 1189.
[6] Labombard, B, Goetz, J, Hutchinson, I, Jablonski, D, Kesner, J, Kurz, C, Lipschultz, B, et al., "Experimental investigation of transport phenomena in the scrape-off layer and divertor", Journal of Nuclear Materials, **241** (1997) 149.
[7] Labombard, B, Umansky, M, Boivin, R, Goetz, J, Hughes, J, Lipschultz, B, Mossessian, D, et al., "Cross-field plasma transport and main-chamber recycling in diverted plasmas on Alcator C-Mod", Nuclear Fusion, **40** (2000) 2041.
[8] Rudakov, D, Boedo, J, Moyer, R, Stangeby, PC, Watkins, J, Whyte, D, Zeng, L, et al., "Far SOL transport and main wall plasma interaction in DIII-D", Nuclear fusion, **45** (2005) 1589.
[9] Whyte, D, Lipschultz, B, Stangeby, P, Boedo, J, Rudakov, D, Watkins, J, West, W, "The magnitude of plasma flux to the main-wall in the DIII-D tokamak", Plasma physics and controlled fusion, **47** (2005) 1579.
[10] Brezinsek, S, Widdowson, A, Mayer, M, Philipps, V, Baron-Wiechec, P, Coenen, J, Heinola, K, et al., "Beryllium migration in JET ITER-like wall plasmas", Nuclear fusion, **55** (2015) 063021.
[11] Behrisch, R, Federici, G, Kukushkin, A, Reiter, D, "Material erosion at the vessel walls of future fusion devices", Journal of Nuclear Materials, **313** (2003) 388.
[12] Mccormick, K, Kyriakakis, G, Neuhauser, J, Kakoulidis, E, Schweinzer, J, Tsois, N, "Particle and energy transport scalings in the ASDEX scrape-off layer", Journal of nuclear materials, **196** (1992) 264.
[13] Lipschultz, B, Whyte, D, Labombard, B, "Comparison of particle transport in the scrape-off layer plasmas of Alcator C-Mod and DIII-D", Plasma Physics and Controlled Fusion, **47** (2005) 1559.
[14] Garcia, OE, Horacek, J, Pitts, RA, Nielsen, AH, Fundamenski, W, Graves, JP, Naulin, V, et al., "Interchange turbulence in the TCV scrape-off layer", Plasma Physics and Controlled Fusion, **48** (2006) L1.
[15] Carralero, D, Birkenmeier, G, Müller, H, Manz, P, Müller, S, Reimold, F, Stroth, U, et al., "An experimental investigation of the high density transition of the scrape-off layer transport in ASDEX Upgrade", Nuclear Fusion, **54** (2014) 123005.
[16] Carralero, D, Müller, H, Groth, M, Komm, M, Adamek, J, Birkenmeier, G, Brix, M, et al., "Implications of high density operation on SOL transport: a multimachine investigation", Journal of Nuclear Materials, **463** (2015) 123.
[17] Militello, F, Garzotti, L, Harrison, J, Omotani, J, Scannell, R, Allan, S, Kirk, A, et al., "Characterisation of the L-mode scrape off layer in MAST: decay lengths", Nuclear Fusion, **56** (2015) 016006.
[18] Labombard, B, Boivin, R, Greenwald, M, Hughes, J, Lipschultz, B, Mossessian, D, Pitcher, C, et al., "Particle transport in the scrape-off layer and its relationship to discharge density limit in Alcator C-Mod", Physics of Plasmas, **8** (2001) 2107.
[19] Umansky, M, Krasheninnikov, S, Labombard, B, Terry, J, "Comments on particle and energy balance in the edge plasma of Alcator C-Mod", Physics of Plasmas, **5** (1998) 3373.
[20] Antar, G, Krasheninnikov, S, Devynck, P, Doerner, R, Hollmann, E, Boedo, J, Luckhardt, S, et al., "Experimental evidence of intermittent convection in the edge of magnetic confinement devices", Physical review letters, **87** (2001) 065001.
[21] Boedo, JA, Rudakov, D, Moyer, R, Krasheninnikov, S, Whyte, D, Mckee, G, Tynan, G, et al., "Transport by intermittent convection in the boundary of the DIII-D tokamak", Physics of Plasmas, **8** (2001) 4826.

[22] Labombard, B, Hughes, JW, Mossessian, D, Greenwald, M, Lipschultz, B, Terry, JL, Alcator, CMT, "Evidence for electromagnetic fluid drift turbulence controlling the edge plasma state in the Alcator C-Mod tokamak", Nuclear Fusion, **45** (2005) 1658.
[23] Garcia, OE, Pitts, R, Horacek, J, Madsen, J, Naulin, V, Nielsen, AH, Rasmussen, JJ, "Collisionality dependent transport in TCV SOL plasmas", Plasma Physics and Controlled Fusion, **49** (2007) B47.
[24] Militello, F, Tamain, P, Fundamenski, W, Kirk, A, Naulin, V, Nielsen, AH, "Experimental and numerical characterization of the turbulence in the scrape-off layer of MAST", Plasma Physics and Controlled Fusion, **55** (2013) 025005.
[25] Garcia, O, "Stochastic modeling of intermittent scrape-off layer plasma fluctuations", Physical review letters, **108** (2012) 265001.
[26] Halpern, FD, Ricci, P, Jolliet, S, Loizu, J, Morales, J, Mosetto, A, Musil, F, et al., "The GBS code for tokamak scrape-off layer simulations", Journal of Computational Physics, **315** (2016) 388.
[27] Krasheninnikov, SI, "On scrape off layer plasma transport", Physics Letters A, **283** (2001) 368.
[28] Kirk, A, Thornton, A, Harrison, J, Militello, F, Walkden, N, Team, M, Team, EM, "L-mode filament characteristics on MAST as a function of plasma current measured using visible imaging", Plasma Physics and Controlled Fusion, **58** (2016) 085008.
[29] Krasheninnikov, S, D'ippolito, D, Myra, J, "Recent theoretical progress in understanding coherent structures in edge and SOL turbulence", Journal of Plasma Physics, **74** (2008) 679.
[30] Myra, J, D’ippolito, D, Stotler, D, Zweben, S, Leblanc, B, Menard, J, Maqueda, R, et al., "Blob birth and transport in the tokamak edge plasma: Analysis of imaging data", Physics of plasmas, **13** (2006) 092509.
[31] Myra, J, Russell, D, D’ippolito, D, "Collisionality and magnetic geometry effects on tokamak edge turbulent transport. I. A two-region model with application to blobs", Physics of plasmas, **13** (2006) 112502.
[32] Carralero, D, Manz, P, Aho-Mantila, L, Birkenmeier, G, Brix, M, Groth, M, Müller, H, et al., "Experimental validation of a filament transport model in turbulent magnetized plasmas", Physical review letters, **115** (2015) 215002.
[33] Vianello, N, Tsui, C, Theiler, C, Allan, S, Boedo, J, Labit, B, Reimerdes, H, et al., "Modification of SOL profiles and fluctuations with line-average density and divertor flux expansion in TCV", Nuclear Fusion, **57** (2017) 116014.
[34] Carralero, D, Madsen, J, Artene, SA, Bernert, M, Birkenmeier, G, Eich, T, Fuchert, G, et al., "A study on the density shoulder formation in the SOL of H-mode plasmas", Nuclear Materials and Energy, **12** (2017) 1189.
[35] Carralero, D, Siccinio, M, Komm, M, Artene, SA, D’isa, FA, Adamek, J, Aho-Mantila, L, et al., "Recent progress towards a quantitative description of filamentary SOL transport", Nuclear Fusion, **57** (2017) 056044.
[36] Angus, JR, Umansky, MV, Krasheninnikov, SI, "Effect of Drift Waves on Plasma Blob Dynamics", Physical Review Letters, **108** (2012) 215002.
[37] Angus, JR, Krasheninnikov, SI, Umansky, MV, "Effects of parallel electron dynamics on plasma blob transport", Physics of Plasmas, **19** (2012) 082312.
[38] Walkden, NR, Dudson, BD, Fishpool, G, "Characterization of 3D filament dynamics in a MAST SOL flux tube geometry", Plasma Physics and Controlled Fusion, **55** (2013) 105005.
[39] Walkden, NR, Dudson, BD, Easy, L, Fishpool, G, Omotani, JT, "Numerical investigation of isolated filament motion in a realistic tokamak geometry", Nuclear Fusion, **55** (2015) 113022.
[40] Militello, F, Walkden, NR, Farley, T, Gracias, WA, Olsen, J, Riva, F, Easy, L, et al., "Multi-code analysis of scrape-off layer filament dynamics in MAST", Plasma Physics and Controlled Fusion, **58** (2016) 105002.

[41] Riva, F, Colin, C, Denis, J, Easy, L, Furno, I, Madsen, J, Militello, F, et al., "Blob dynamics in the TORPEX experiment: a multi-code validation", Plasma Physics and Controlled Fusion, **58** (2016) 044005.
[42] Walkden, NR, Wynn, A, Militello, F, Lipschultz, B, Matthews, G, Guillemaut, C, Harrison, J, et al., "Interpretation of scrape-off layer profile evolution and first-wall ion flux statistics on JET using a stochastic framework based on fillamentary motion", Plasma Physics and Controlled Fusion, **59** (2017) 085009.
[43] Wersal, C, Ricci, P, "A first-principles self-consistent model of plasma turbulence and kinetic neutral dynamics in the tokamak scrape-off layer", Nuclear Fusion, **55** (2015) 123014.
[44] Matthews, GF, Edwards, P, Hirai, T, Kear, M, Lioure, A, Lomas, P, Loving, A, et al., Overview of the ITER-like Wall Project in: 11th International Workshop on Plasma-Facing Materials and Components for Fusion Applications, Greifswald, Germany, 2006.
[45] Wynn, A, Lipschultz, B, Matthews, G, Tal, B, Militello, F, Walkden, N, Guillemaut, C, et al., Radial fluxes and density shoulder formation in the scrape off layer of JET, in: 22nd International Conference on Plasma Surface Interaction in Controlled Fusion Devices, Rome, 2016, pp. P2.46.
[46] Militello, F, Omotani, J, "Scrape off layer profiles interpreted with filament dynamics", Nuclear Fusion, **56** (2016) 104004.
[47] Brix, M, Dodt, D, Korotkov, A, Morgan, P, Dunai, D, Fischer, R, Meigs, A, et al., "Upgrade of the lithium beam diagnostic at JET", Review of Scientific Instruments, **81** (2010) 10D733.
[48] Huber, A, Brezinsek, S, Mertens, P, Schweer, B, Sergienko, G, Terra, A, Arnoux, G, et al., "Development of a mirror-based endoscope for divertor spectroscopy on JET with the new ITER-like wall (invited)", Review of Scientific Instruments, **83** (2012) 10D511.
[49] Silburn, S, Calcam, https://github.com/euratom-software/calcam
[50] Atomic Data and Analysis Structure, http://open.adas.ac.uk/
[51] Harrison, J., Image inversion analysis, https://git.ccfe.ac.uk/jrh/kl11
[52] Horacek, J, Pitts, RA, Stangeby, PC, Batishchev, O, Loarte, A, "Predicted effects of parallel temperature gradients on the overestimation of TCV divertor target Langmuir probe Te measurements", Journal of Nuclear Materials, **313** (2003) 931.
[53] Lipschultz, B, Goetz, J, Hutchinson, I, Labombard, B, Mccracken, G, Takase, K, Terry, JL, et al., Variation of the divertor geometry in Alcator C-Mod, in: 14th Int. Conf. on Plasma Physics and Controlled Fusion Research, IAEA, Vienna (1997), Montreal, 1996.
[54] Lipschultz, B, Labombard, B, Terry, JL, Boswell, C, Hutchinson, IH, "Divertor physics research on Alcator C-Mod", Fusion Science and Technology, **51** (2007) 369.
[55] Loarte, A, "Effects of divertor geometry on tokamak plasmas", Plasma Physics & Controlled Fusion, **43** (2001).
[56] Oberkofler, M, Douai, D, Brezinsek, S, Coenen, JW, Dittmar, T, Drenik, A, Romanelli, SG, et al., "First nitrogen-seeding experiments in JET with the ITER-like Wall", Journal of Nuclear Materials, **438** (2013) S258.
[57] Fuchert, G, Carralero, D, Manz, P, Stroth, U, Wolfrum, E, Team, AU, "Towards a quantitative prediction of the blob detection rate", Plasma Physics and Controlled Fusion, **58** (2016) 054006.
[58] Field, AR, Balboa, I, Drewelow, P, Flanagan, J, Guillemaut, C, Harrison, JR, Huber, A, et al., "Dynamics and stability of divertor detachment in H-mode plasmas on JET", Plasma Physics and Controlled Fusion, **59** (2017) 095003.
[59] Giroud, C, Jachmich, S, Jacquet, P, Järvinen, A, Lerche, E, Rimini, F, Aho-Mantila, L, et al., "Progress at JET in integrating ITER-relevant core and edge plasmas within the constraints of an ITER-like wall", Plasma Physics and Controlled Fusion, **57** (2015) 035004.
[60] Militello, F, Omotani, J, "On the relation between non-exponential scrape off layer profiles and the dynamics of filaments", Plasma Physics and Controlled Fusion, **58** (2016) 125004.
[61] Lipschultz, B, Labombard, B, Pitcher, C, Boivin, R, "Investigation of the origin of neutrals in the main chamber of Alcator C-Mod", Plasma physics and controlled fusion, **44** (2002) 733.

[62] Stangeby, PC, "Modeling plasma contact with the main vessel walls of a divertor tokamak", Physics of Plasmas, **9** (2002) 3489.

[63] Lipschultz, B, Andrew, P, Coad, J, Erents, SK, Felton, R, Fundamenski, W, Hidalgo, C, et al., A study of JET radial transport based on particle balance, in: 30th European Conf. On Controlled Fusion and Plasma Physics, European Physical Society, Geneva, St. Petersburg, Russia, 2003.

[64] Jaervinen, AEU, Brezinsek, S, Giroud, C, Groth, M, Guillemaut, C, Belo, P, Brix, M, et al., "Impact of divertor geometry on radiative divertor performance in JET H-mode plasmas", Plasma Physics and Controlled Fusion, **58** (2016).

[65] Cooke, PIH, Prinja, AK, "An analytic model for flow reversal in divertor plasmas", Nuclear Fusion, **27** (1987) 1165.

[66] Asakura, N, "Understanding the SOL flow in L-mode plasma on divertor tokamaks, and its influence on the plasma transport", Journal of Nuclear Materials, **363** (2007) 41.

[67] Schneider, R, Bosch, HS, Coster, D, Fuchs, JC, Gafert, J, Haas, G, Herrmann, A, et al., "Role of divertor geometry on detachment in ASDEX Upgrade", Journal of Nuclear Materials, **266–269** (1999) 175.

[68] Boedo, JA, Porter, GD, Schaffer, MJ, Lehmer, R, Moyer, RA, Watkins, JG, Evans, TE, et al., "Flow reversal, convection, and modeling in the DIII-D divertor", Physics of Plasmas, **5** (1998) 4305.

[69] Schneider, R, Bonnin, X, Borrass, K, Coster, D, Kastelewicz, H, Reiter, D, Rozhansky, V, et al., "Plasma Edge Physics with B2-Eirene", Contributions to Plasma Physics, **46** (2006) 3.

[70] Hidalgo, C, Gonçalves, B, Silva, C, Pedrosa, M, Erents, K, Hron, M, Matthews, G, "Experimental investigation of dynamical coupling between turbulent transport and parallel flows in the JET plasma-boundary region", Physical review letters, **91** (2003) 065001.

[71] Chankin, AV, Delabie, E, Corrigan, G, Maggi, CF, Meyer, H, Contributors, JET, "Possible influence of near SOL plasma on the H-mode power threshold", Nuclear Materials and Energy, **12** (2017) 273.

[72] Militello, F, Fundamenski, W, Naulin, V, Nielsen, AH, "Simulations of edge and scrape off layer turbulence in mega ampere spherical tokamak plasmas", Plasma Physics and Controlled Fusion, **54** (2012) 095011.

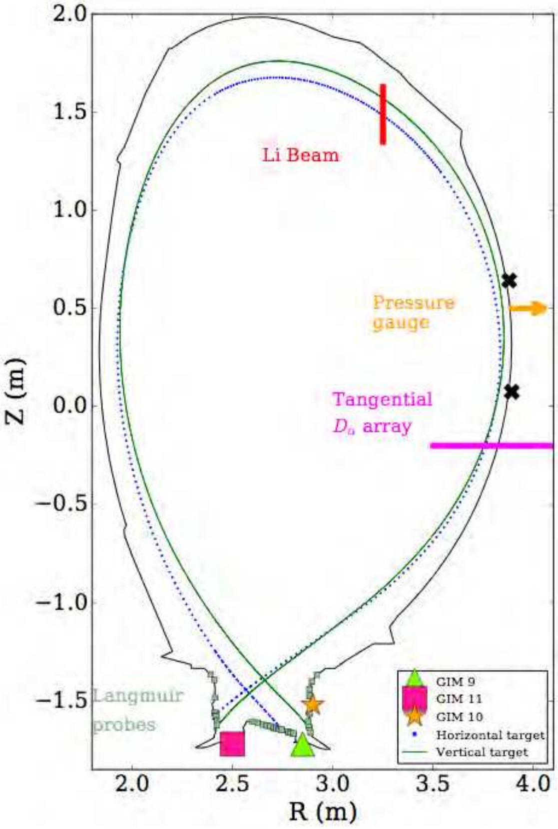

Figure 1: Diagnostics and gas injection module (GIMs) locations used in the study are shown with the magnetic equilibrium of the vertical and horizontal target divertor configurations.

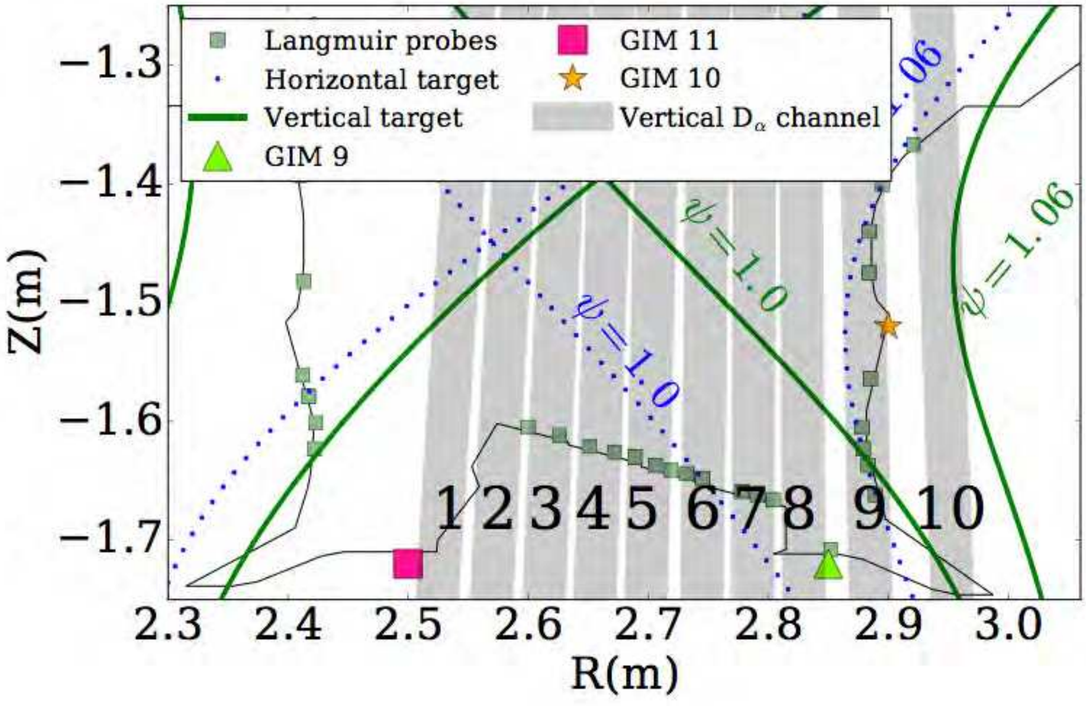

Figure 2: Close up of the divertor region of Fig. 1, showing the locations of the vertical viewing D_α channels, Langmuir probes, Gas Injection Modules (GIMs) and the vertical and horizontal targets equilibria.

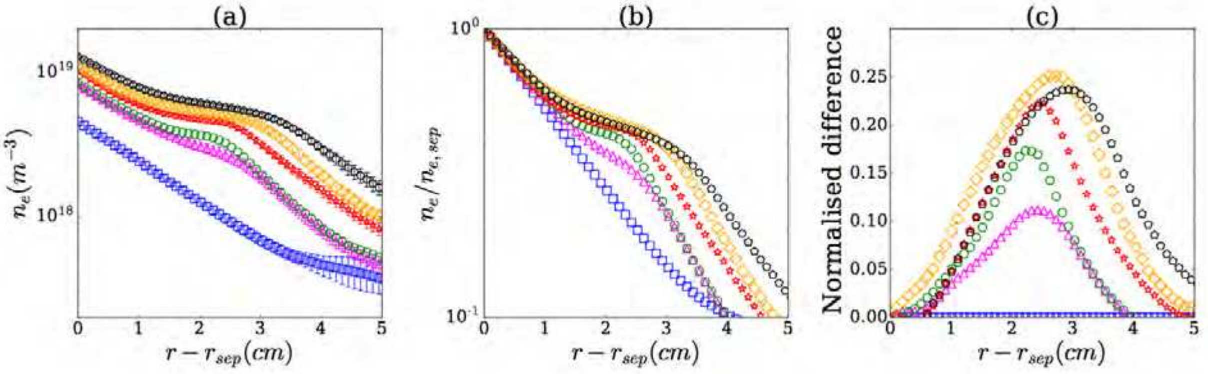

Figure 3: (a) Example density profiles during a horizontal target L-mode D fuelling ramp (JPN 89346) showing characteristic flattening. (b) The same density profiles normalised to separatrix radius. (c) Normalised difference profiles calculated by subtracting the reference profile (blue squares) from a given profile. The horizontal coordinate, r-r_{sep}, is the distance from the separatrix radius, mapped to the midplane.

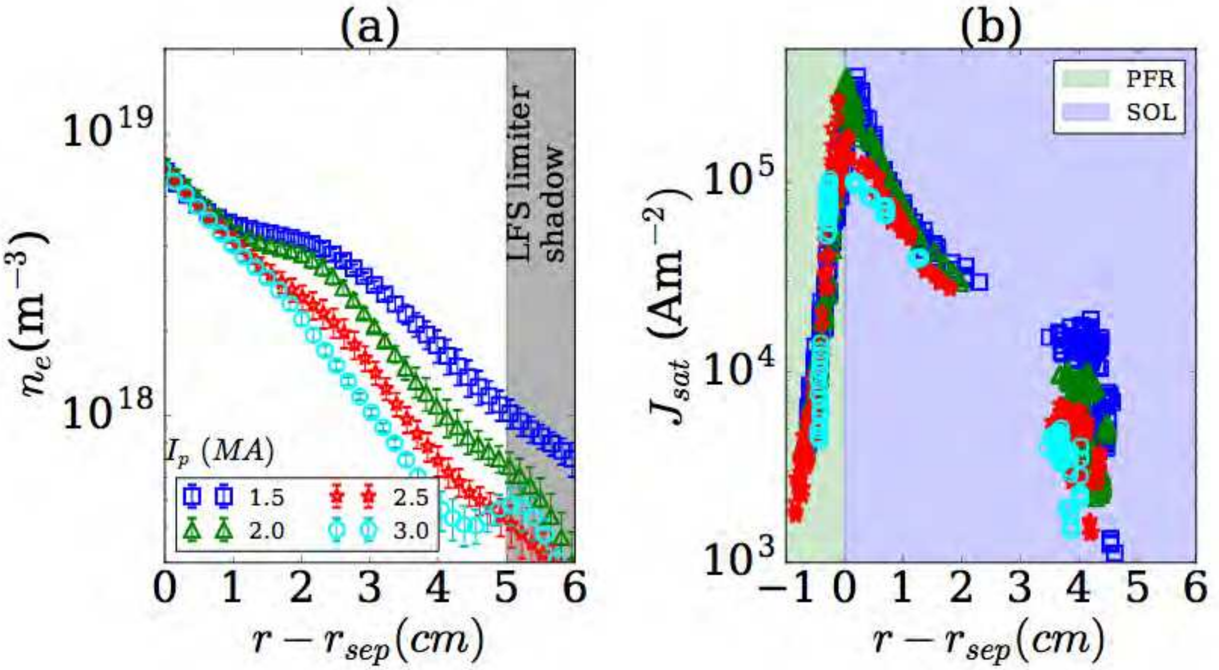

Figure 4: (a) Upstream density profiles for a fixed $\bar{n}_e$ for a range of plasma current, I_p and toroidal field (the toroidal magnetic field is matched to the current to keep the safety factor, q, constant). (b) Corresponding change to the outer horizontal divertor J_{sat} profile. All profiles are mapped back to mid plane in terms of distance to the separatrix. The profiles shown are averaged over 10 measurement periods. The error bars are the standard deviation of those measurements. The diagnostic signal to noise ratio near the limiter is of order 1 at the lowest densities there and thus the deviation from the exponential for the 3MA case is not significant. The pulse numbers are JPN893(44,50,46,48) ordered with increasing I_p.

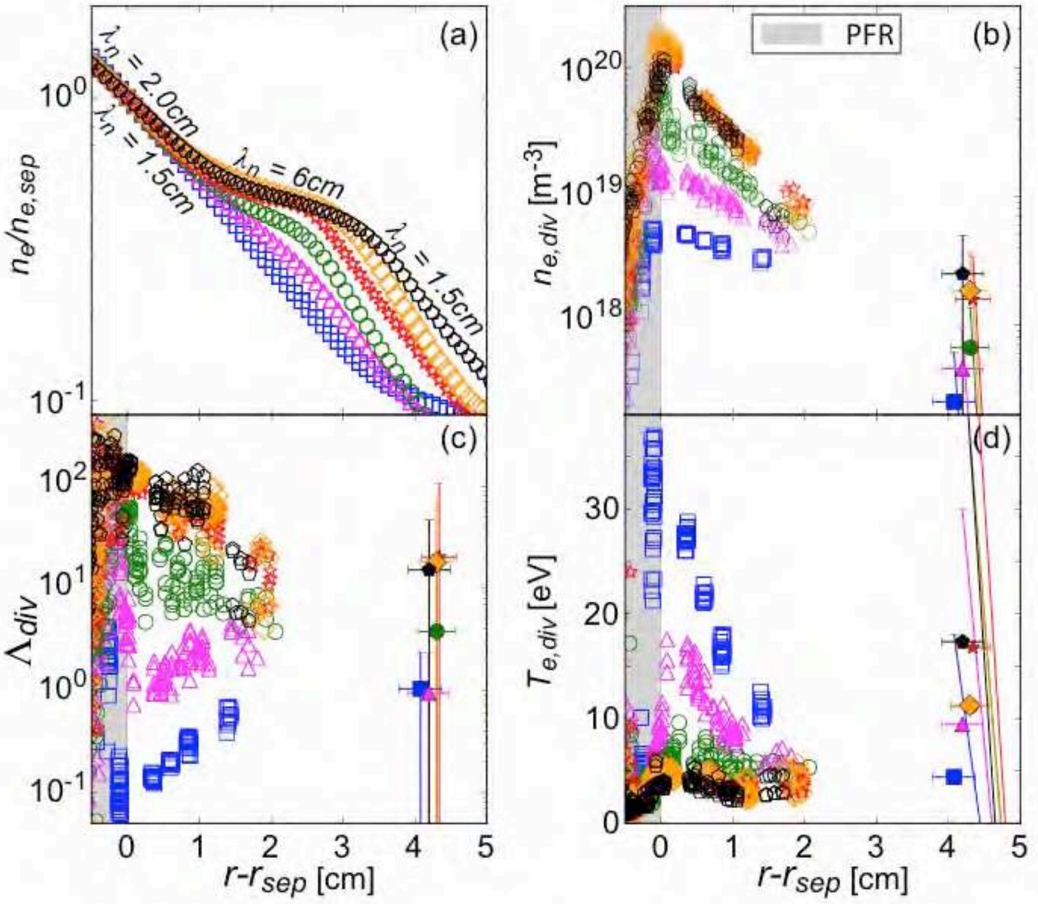

Figure 5: Horizontal target D fuelling ramp for a 2.5MA plasma (JPN89346): (a) normalized SOL density profiles showing the formation and growth of the shoulder. (b) Divertor target density profiles showing the transition from SL (blue squares) to peak HR (red stars), as the divertor becomes more high-recycling (green circles, red stars, orange diamonds) and detachment onset (black pentagons) (c) The resultant change to Λ_{div}; (d) Divertor T_e profiles. Limiter radius ~ $r-r_{sep}$~ 5 cm. Colour and symbols correspond to figure 6.

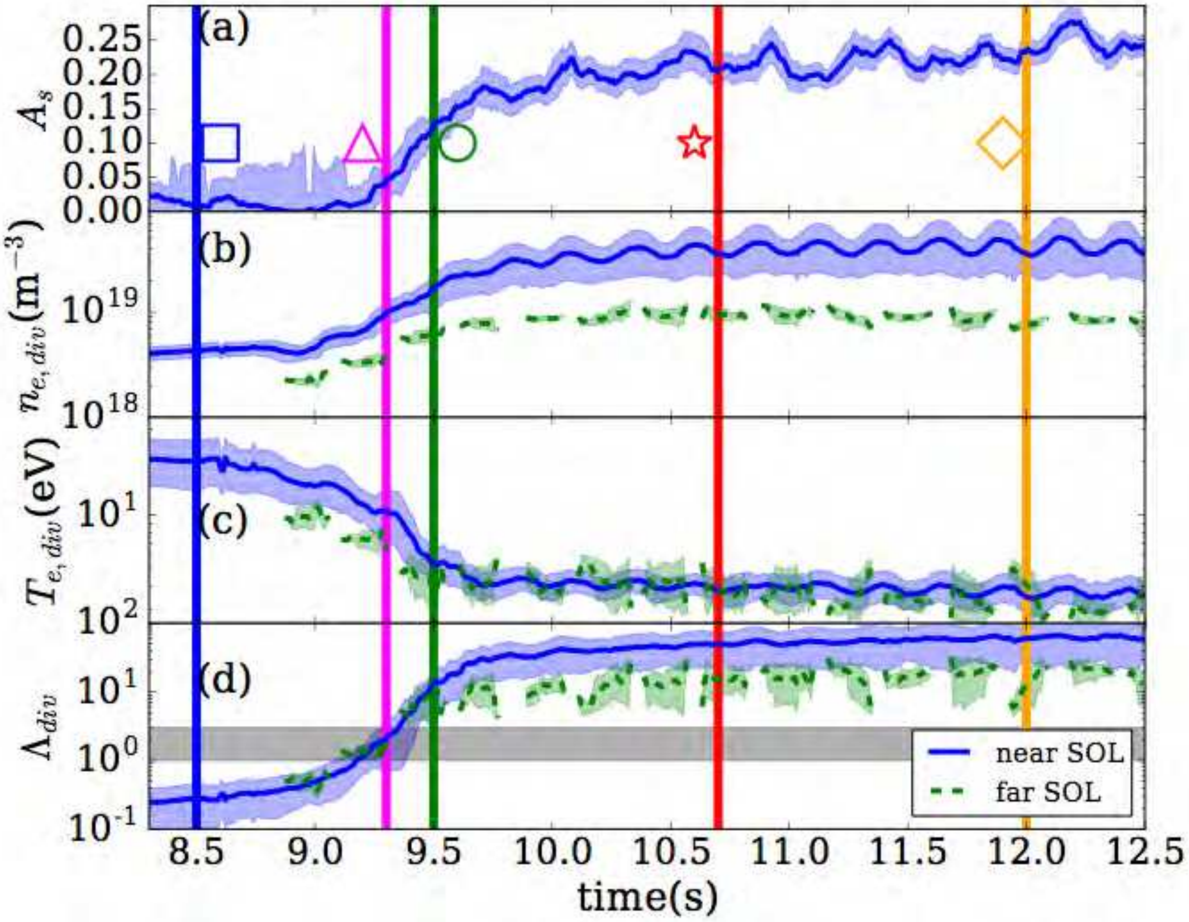

Figure 6: Time traces of quantities shown in figure 5 (JPN89346); vertical lines with symbols and colors correspond to the times of the profiles given in Fig. 5. The normalized shoulder amplitude, A_s is given in (a); (b) and (c) are the evolution of the density and temperature averaged over near ($r-r_{sep}$ = 0-1.5cm) and far ($r-r_{sep}$ = 1.5-3cm) SOL, referenced to the midplane; d) gives the divertor resistivities, $\Lambda_{div,near}$ and $\Lambda_{div,far}$, calculated using the data from (b) and (c). Gaps in data for far SOL are due to strike point sweeping and probe spacing.

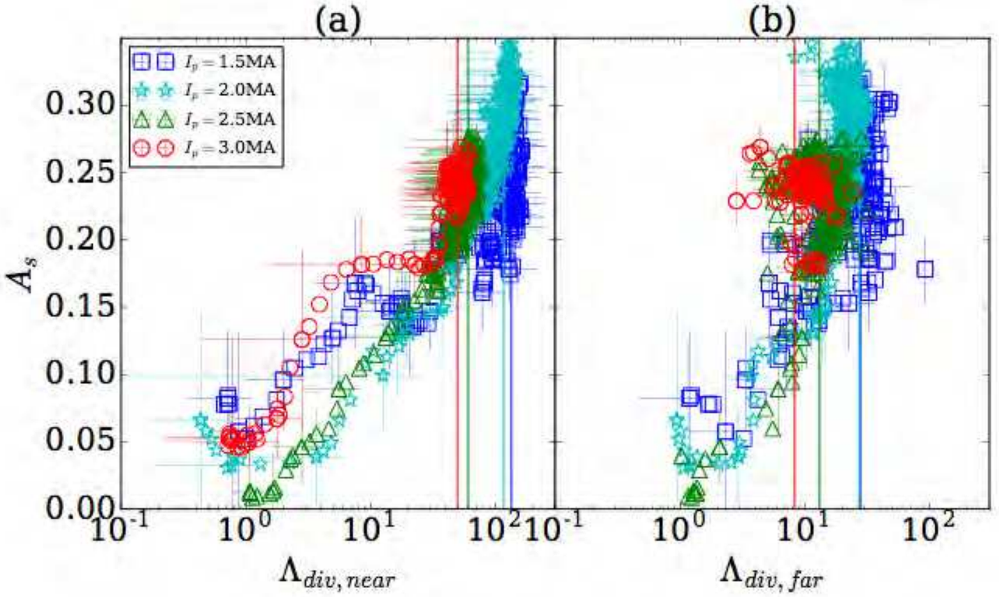

Figure 7: The shoulder amplitude, A_s, vs Λ_{div}, averaged over (a) near (r-r_{sep} = 0-1.5cm) and (b) far (r-r_{sep} = 1.5-3 cm) SOL regions for the 4 plasma currents given in legend. All cases are L-mode, horizontal target plasmas, and D_2 puffing driving a core density ramp. Vertical lines indicate the onset of detachment for corresponding colours. The error bars are representative of the standard deviation of the data in the specified regions (near and far SOL) over 0.1s. Pulse numbers are JPN893(44,50,46,48) ordered with increasing I_p.

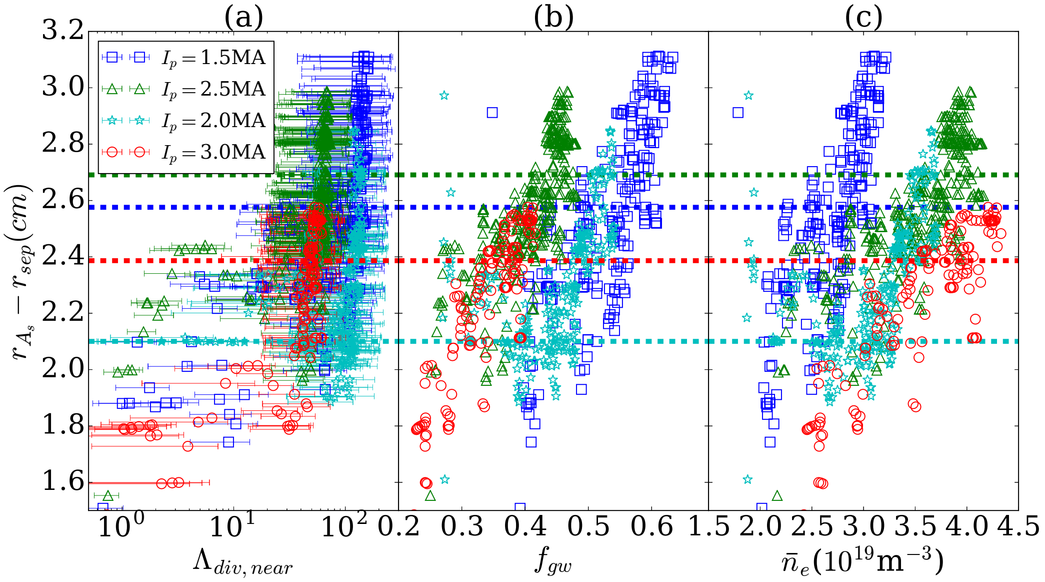

Figure 8: Movement of the radial location of A_s r_{As}, as a function of Λ_{div}:(a), $\bar{n}_e$ /n$_{gw}$ (b) and $\bar{n}_e$ (c) for the 4 plasma currents of Fig. 5 with L-mode, horizontal target plasmas and D_2 puffing driving a core density ramp. (a) indicates the 2 phases of the profile evolution, initial formation/growth followed by expansion (increasing radius of the peak of the shoulder, r_{As}). Horizontal lines indicate the onset of detachment for each plasma current.

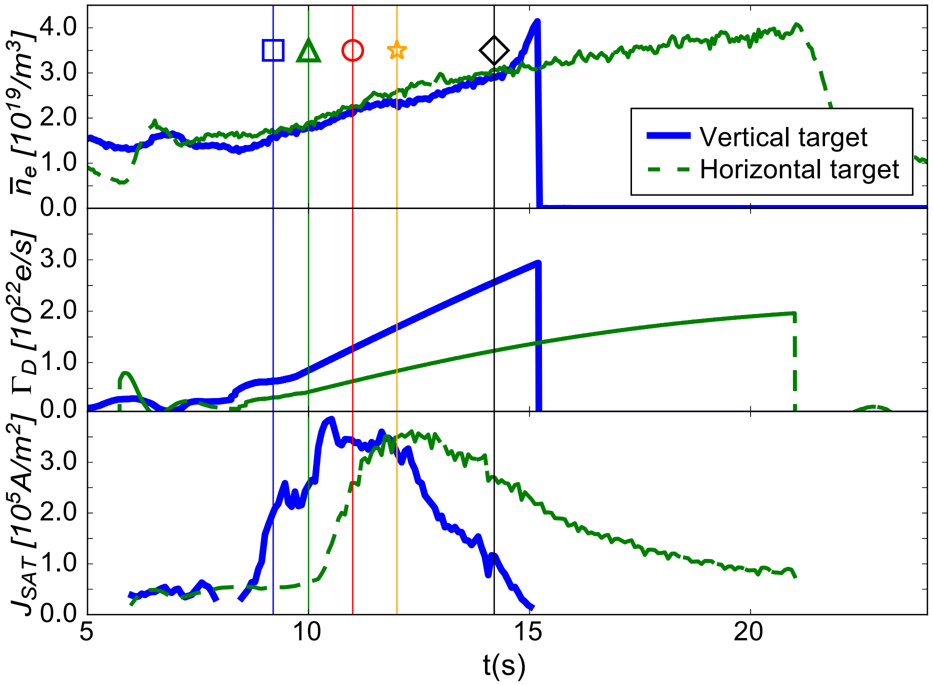

Figure 9: Time traces of for vertical (JPN 89782) and horizontal (JPN 89344) target L-mode D fuelling ramps at 1.5 MA. Shown are (a) $\bar{n}_e$, Γ_D (b), and strike point J$_{sat}$,(c). Detachment is evident in the rollover in J$_{sat}$. Vertical lines marked with symbols indicate times used for VT profiles shown in figure 10. More gas is needed to achieve the same $\bar{n}_e$ for the case of the strike point on the vertical target.

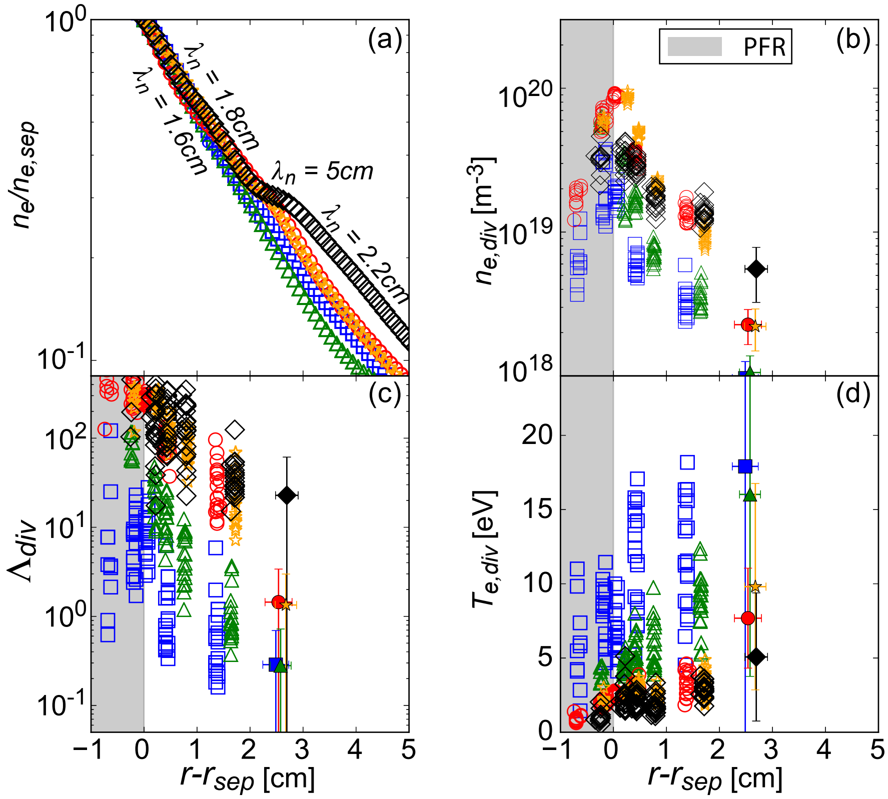

Figure 10: (a) Upstream density profiles, divertor probe data (b & d) and Λ_{div} (c) for a vertical target 1.5MA plasma utilizing a D_2-fuelling ramp to increase $\bar{n}_e$ (JPN89782). The divertor condition (SL, HR or detached) is different in the near vs far SOL. Colors and symbols correspond to figure 9.

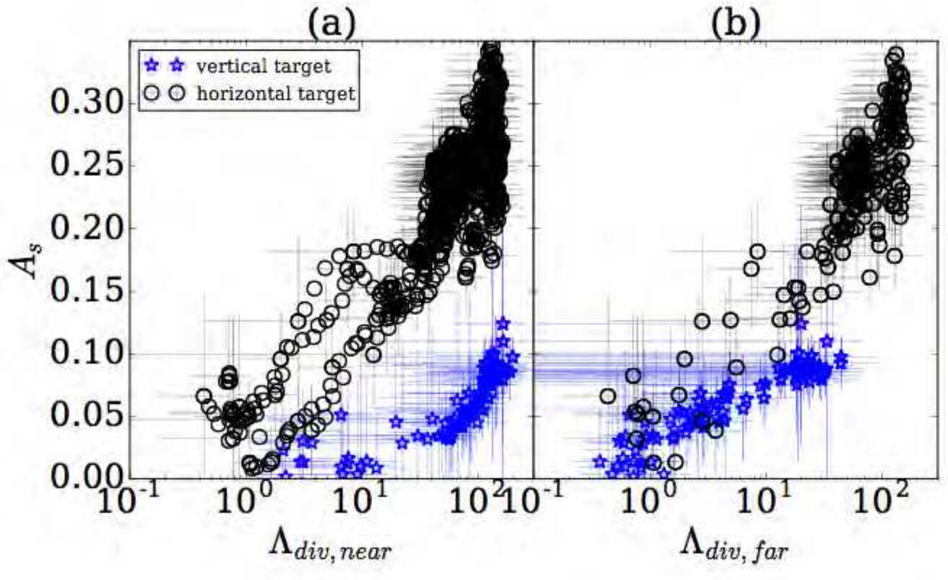

Figure 11: The data is from the same 1.5MA, vertical divertor pulse (JPN89782) as Fig. 10. The correlation between the shoulder amplitude A_s and Λ_{div} in the near (a) and far (b) SOL is given. The data from figure 7 (labeled horizontal target, JPN89344) is also shown for reference.

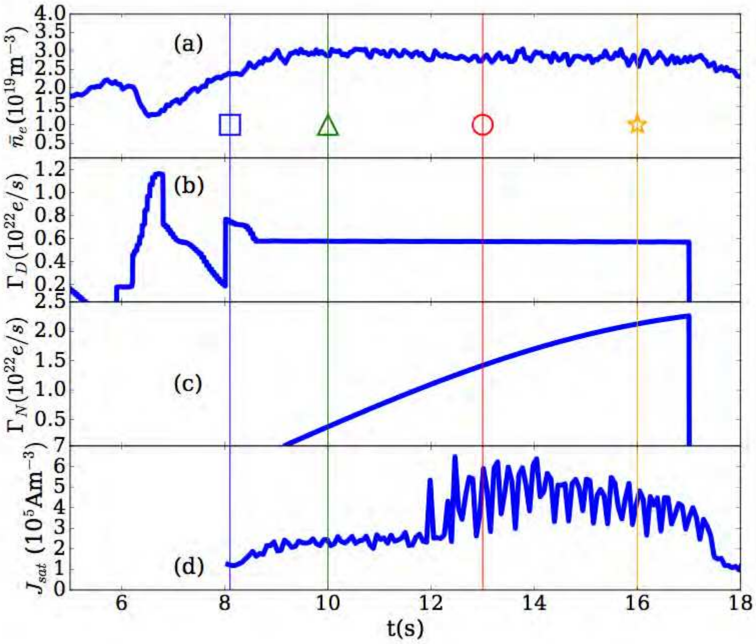

Figure 12: Time traces of N seeding ramps showing (a) $\bar{n}_e$, (b) D_2 fuelling rate, Γ_D (c) N_2 seeding rate, Γ_N, and strike point current density, J_{sat}. Ip = 2.5MA (JPN90697). Colored vertical lines marked with symbols correspond to figure 13.

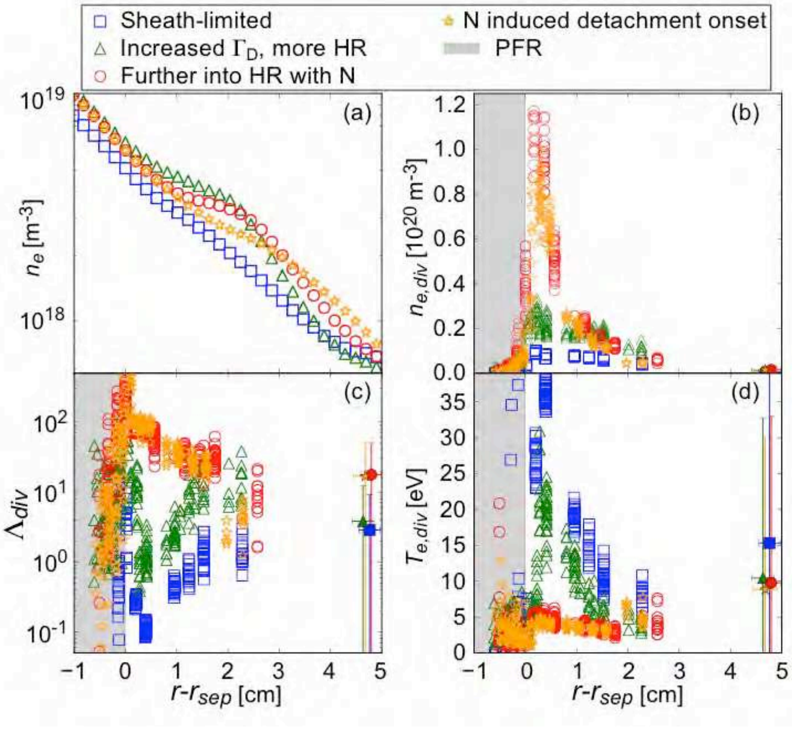

Figure 13: (a) Upstream density profiles, divertor probe data (b, d) and Λ_{div} (d) for a horizontal target N_2 seeding ramp and constant core density, I_p = 2.5MA (JPN90697). Despite strong changes to the divertor conditions due to N_2 seeding, there is only minimal change to the upstream density profile. See Figure 5 for comparison D_2 fuelled case.

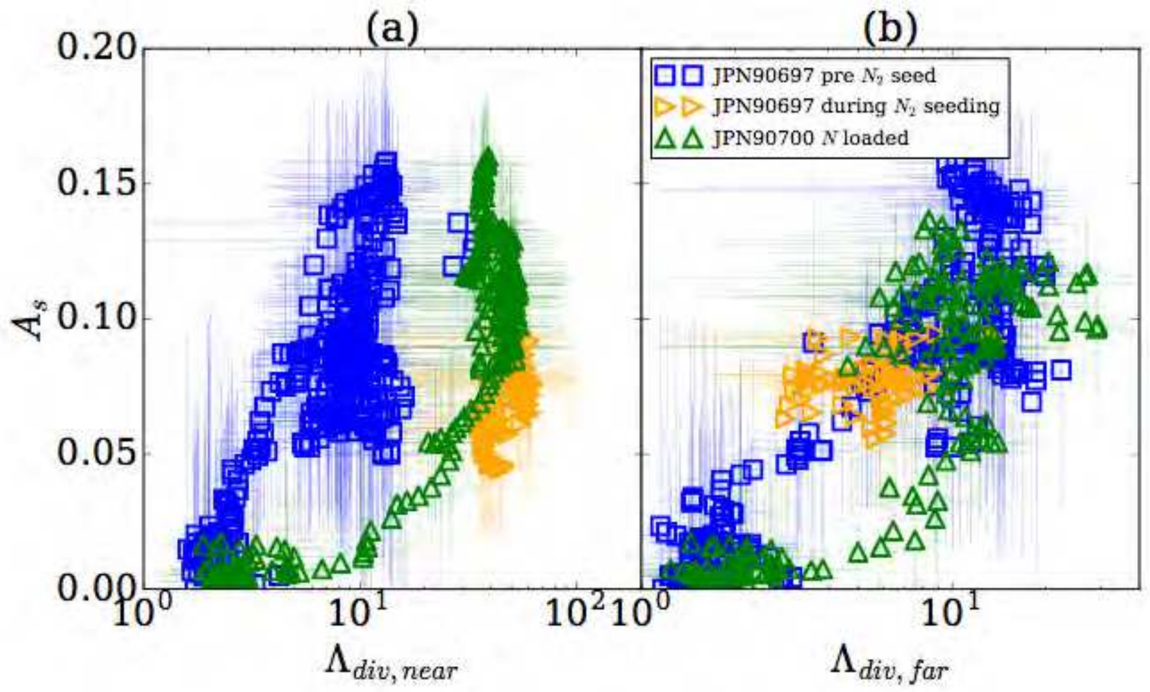

Figure 14: Correlation between the shoulder amplitude A_s and Λ_{div} in the near (a) and far (b) SOL for horizontal target N_2-seeded pulses. Data JPN90700 is for N_2-loaded walls

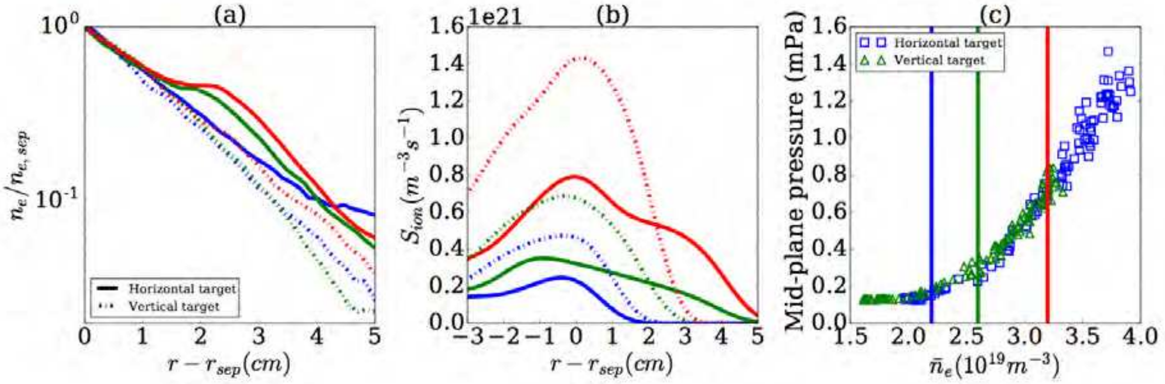

Figure 15: (a) Comparison of normalized density profiles from horizontal (JPN89346) and vertical target (JPN89783) discharges. Colors correspond to specific line-averaged densities as indicated by vertical lines in (c).

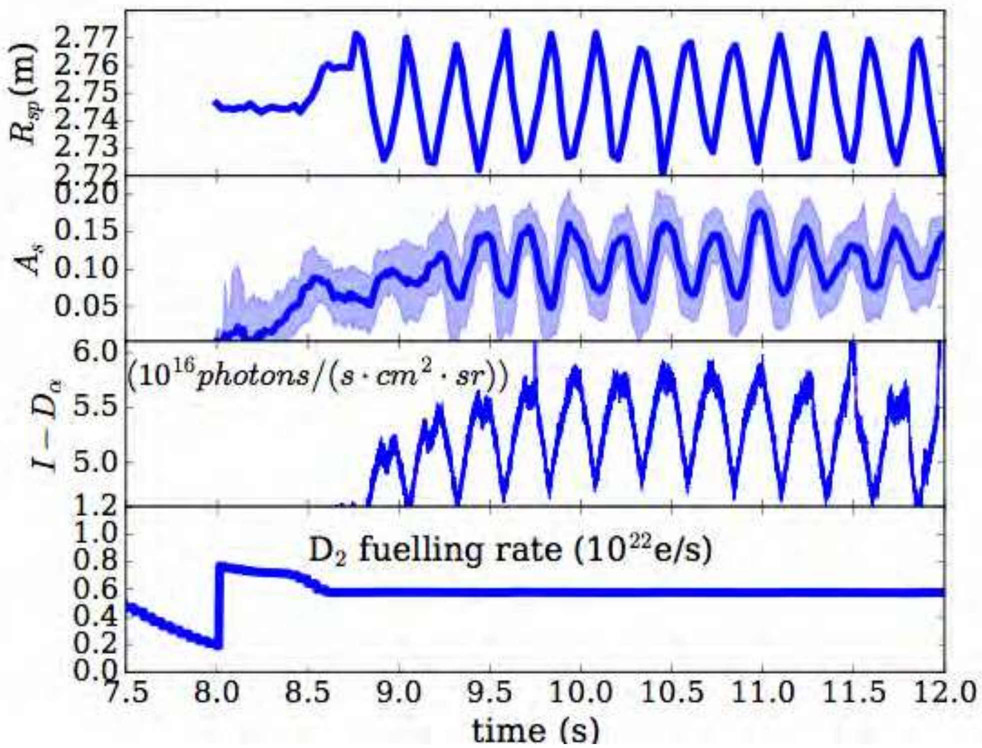

Figure 16: Effect of strike point sweeping on the shoulder amplitude and the outer target D_α emission during period when the line-averaged density is constant and the N_2-seeding has not affected the divertor. Data from JPN90697 (also shown in Figures 12 &13). I-D_α is the sum over vertical D_α chords C3-C7 (see Fig. 2)

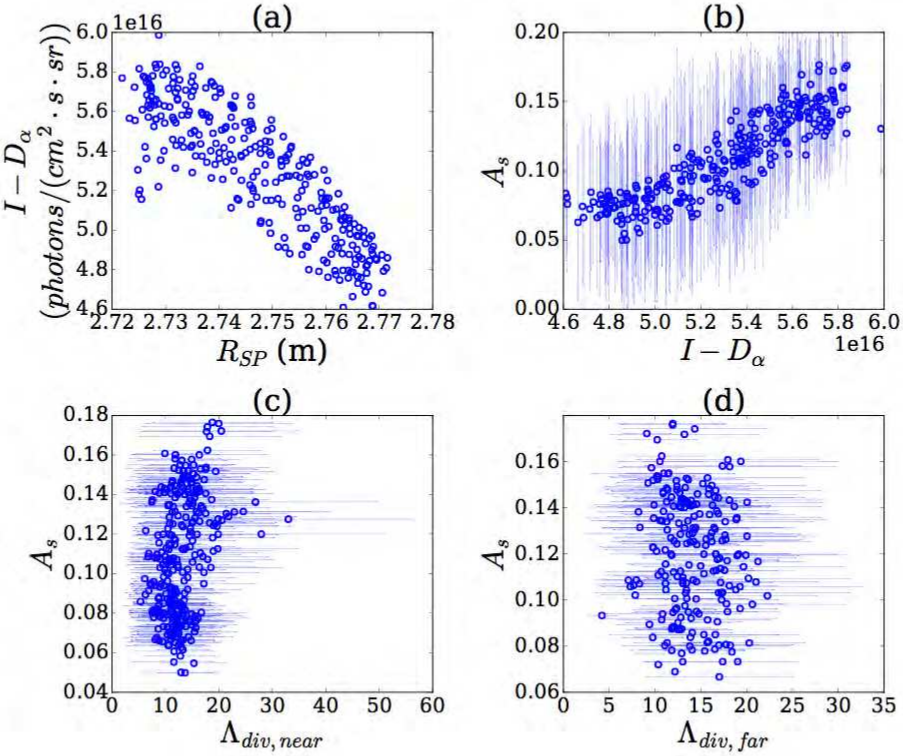

Figure 17: Correlation between the upstream SOL shoulder amplitude, A_s, and divertor characteristics over the period 9-12s of pulse JPN90697. The divertor is in a high recycling condition.

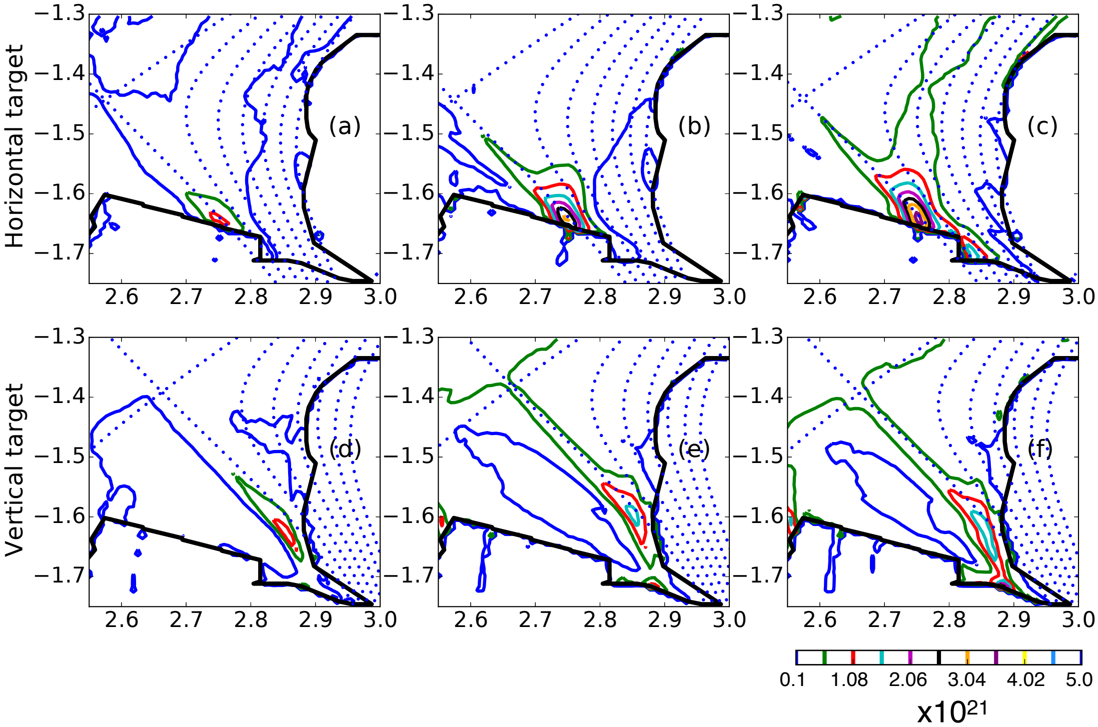

Figure 18: D_α emission contours for horizontal (top row JPN89346, also shown in Fig. 6) and vertical (bottom row JPN89355) divertor targets. Core densities increase from left to right and are equivalent for each column, the values of which are indicated by vertical lines in figure 15 (c). (a,d) Sheath limited conditions, no shoulder. (b,e) High-recycling conditions with shoulder formation for the horizontal target; (c,f) Divertor conditions are at maximum high-recycling, just before detachment; shoulder $A_s = 0.22$ for the horizontal target, no measurable shoulder for the vertical target. Flux surfaces are dotted and are separated in normalized flux Ψ by 0.01 ($\Psi_{sep} = 1$). The uncertainty in the absolute location of D_α contours is estimated to be 2-3cm and is due to uncertainties in mapping optical camera pixels to vessel structures and in equilibrium reconstruction.

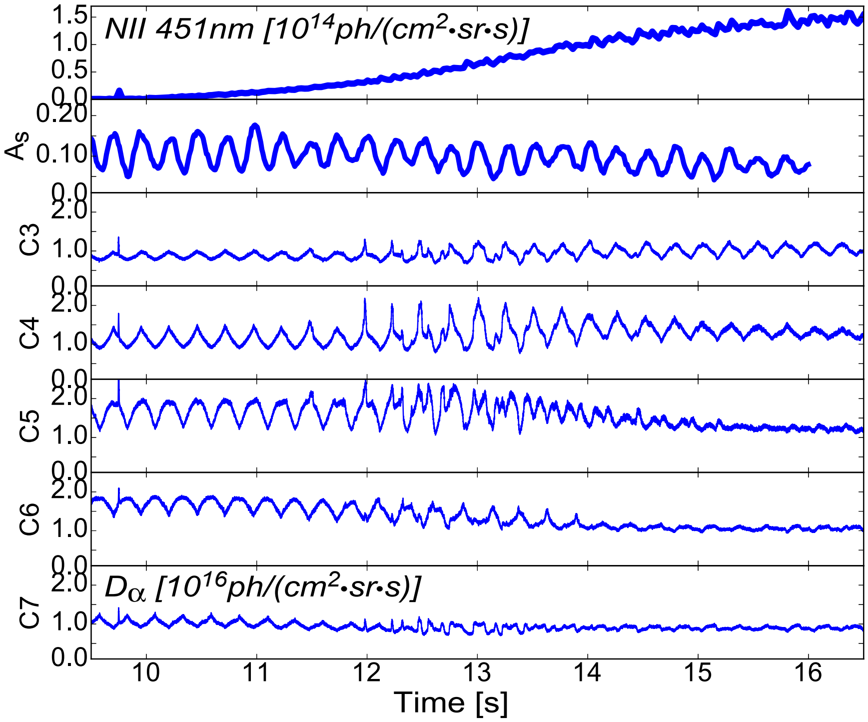

Figure 19: Time traces of (a) NII brightness, (b) Shoulder amplitude A_s and vertical views of the horizontal target (C3-7) in D_α brightness are given for JPN90697. The direction of increasing R across the target is C3 to C7. D_2 fuelling is constant over the period shown. The same pulse is also described in Figures 12 and 16.

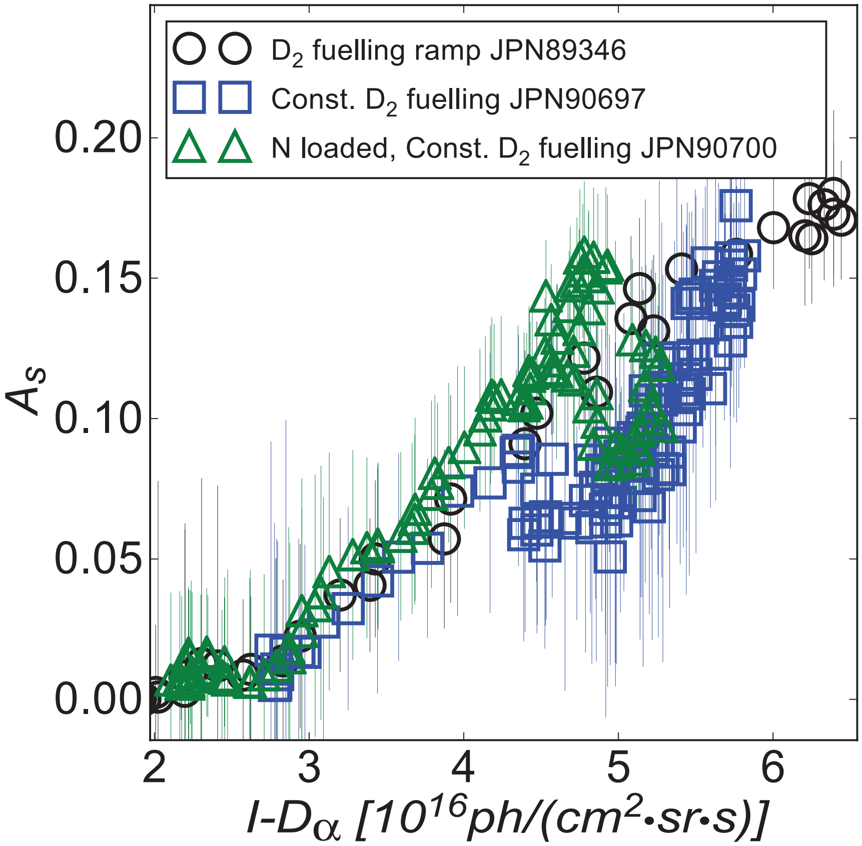

Figure 20: Correlation between I-D_α and A_s for several discharges utilizing the horizontal target. Black circles are for a 2.5 MA D_2 fuelling ramp case (JPN89346, also shown in Fig. 7). Blue squares are from 2 constant D_2 fuelling (and density) cases with strike point sweeping (shown with same symbols and colors in Fig. 14): JPN90697 – prior to N_2 seeding; JPN90700 – walls loaded with N.

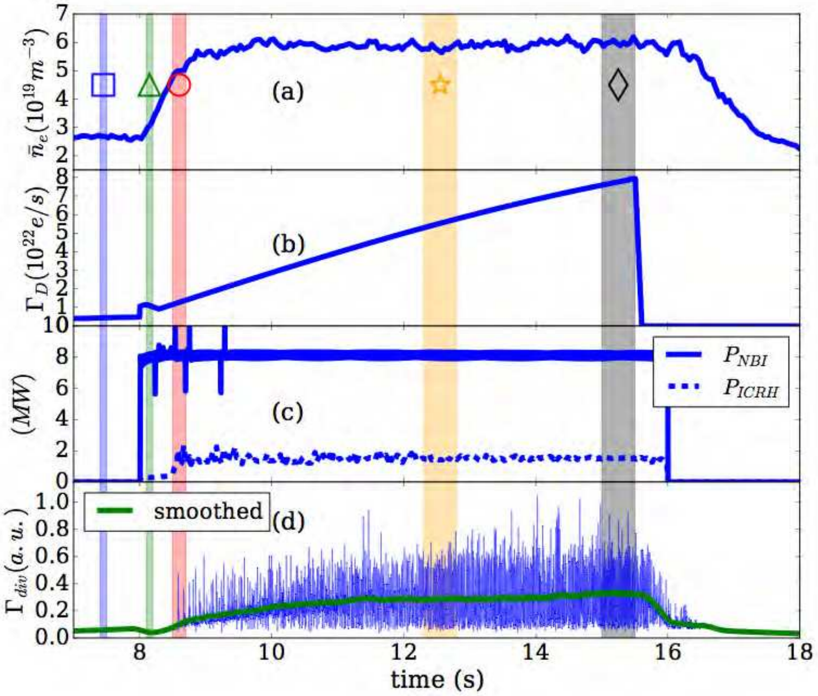

Figure 21: Time traces for a horizontal target D_2 fuelling ramp H-mode (JPN 89786, I_p = 2.2MA). (a) $\bar{n}_e$ (b) D_2 fuelling rate. Additional heating power from NBI and ICRH (c). Raw and smoothed flux to the outer divertor, Γ_{div} (d). Shaded regions marked with symbols indicate times from which inter-ELM profiles are taken. Symbols correspond to figure 23.

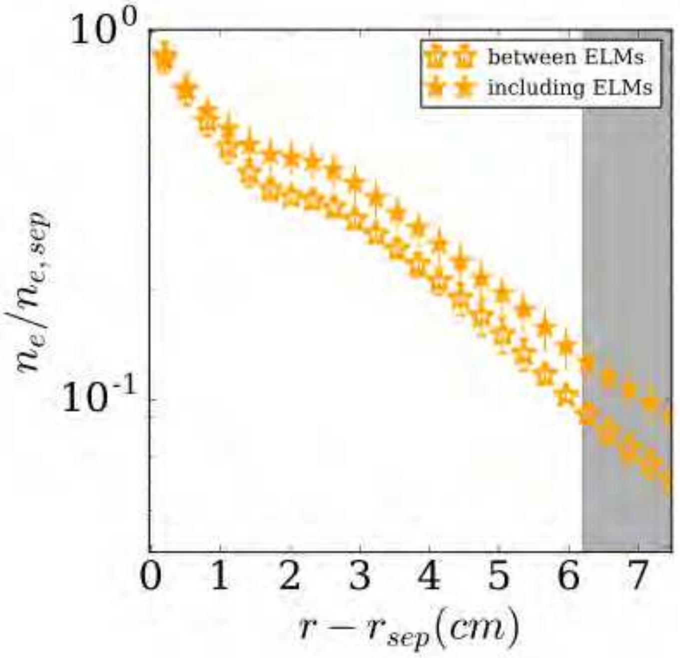

Figure 22: Normalised density profiles averaged over measurements which are either between ELMs or include ELM contributions. The time window over which profiles are taken is shown in figure 21 with corresponding symbols (JPN89786).

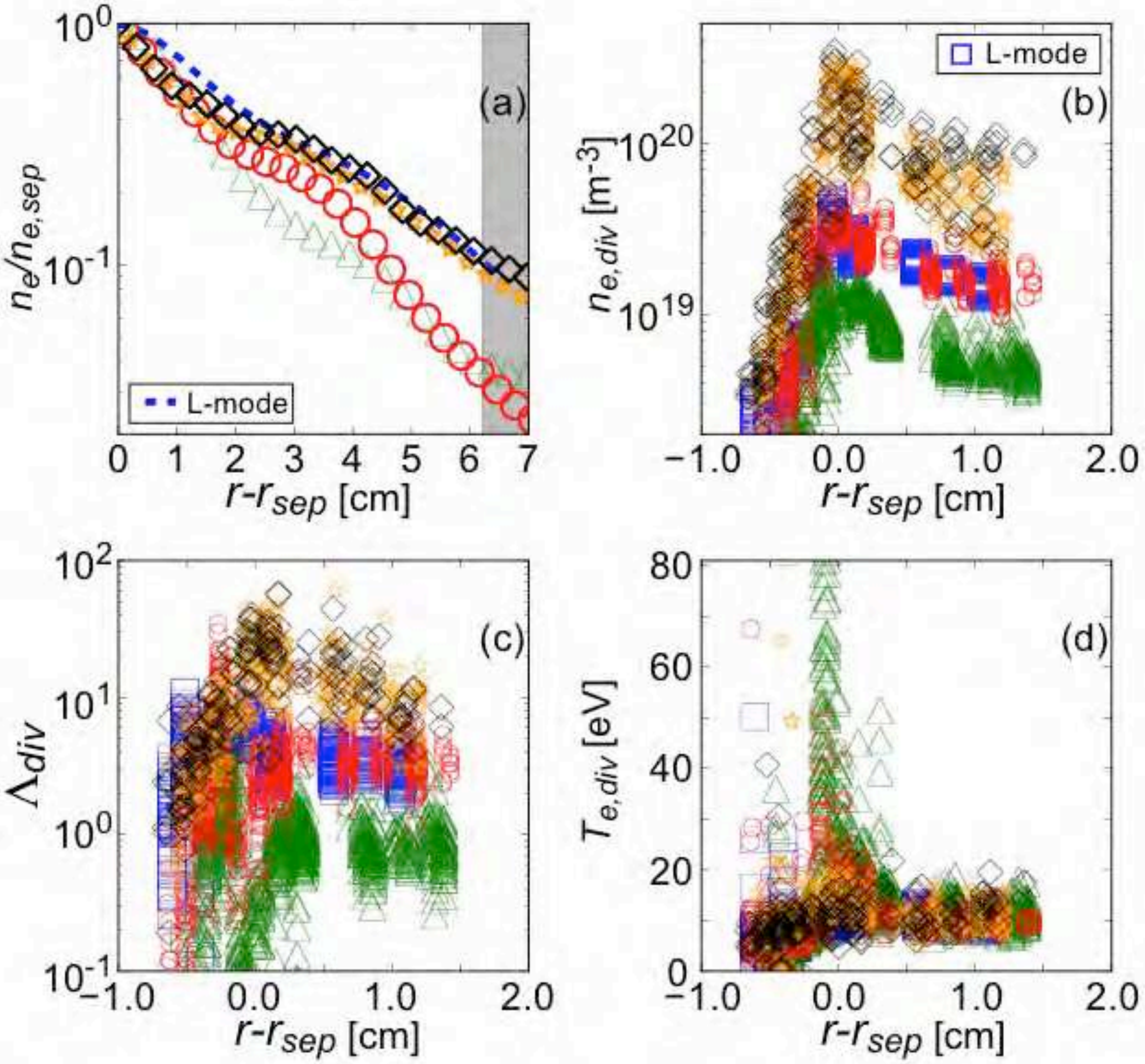

Figure 23: Upstream density profiles (a) and divertor probe data (b,d) along with Λ_{div} (c) for a horizontal target H-mode D fuelling ramp (JPN 89786, I_p = 2.5MA). L-mode data (blue dashed line or squares) is shown for reference. All H-mode profiles are from inter-ELM periods. The probe data has been shifted by +0.25cm such that the peak is at the separatrix. Divertor conditions change from SL to HR, but detachment does not occur. Λ_{div} follows the profile evolution from L-mode to H-mode. Symbols correspond to figure 21.

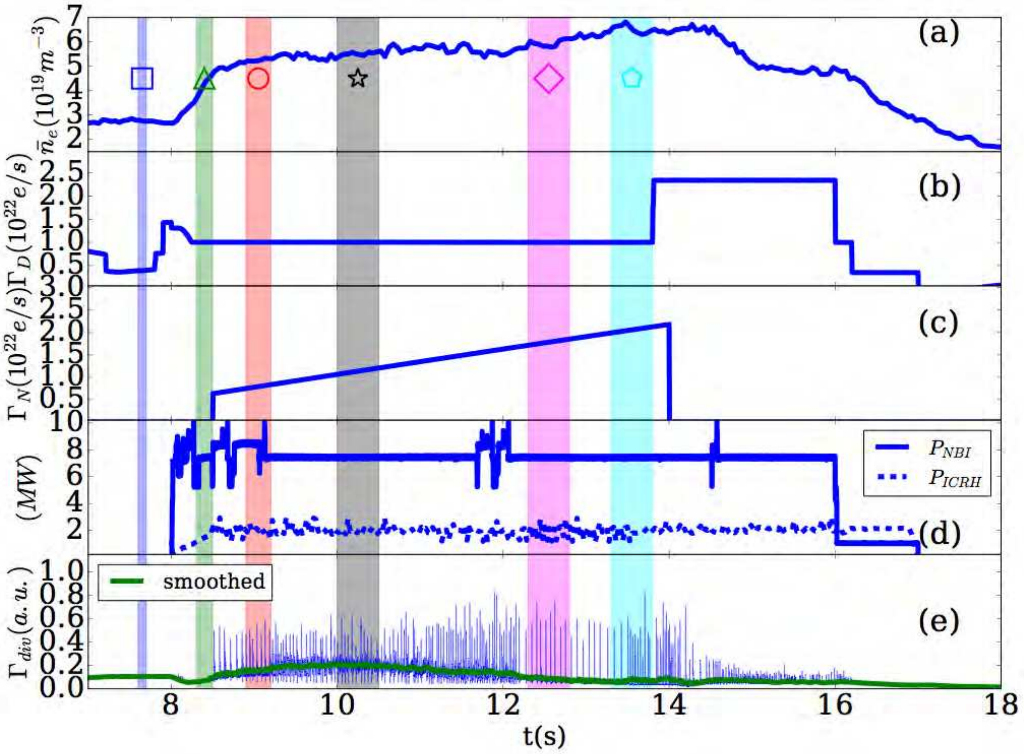

Figure 24: Time traces for a horizontal target H-mode N seeding ramp (JPN 89241,I_p = 2.0MA). Shaded regions marked with symbols indicate times from which inter-ELM profiles are selected. $\overline{n}_e$ (a) increases at transition to detached conditions (magenta diamonds) and onwards (cyan pentagons). The D_2-fuelling rate (b), Γ_D, is shown along with the N_2-seeding rate, Γ_N (c). Additional heating power from NBI and ICRH (d) are shown along with the total flux to the outer divertor (e), Γ_{div}, which drops during detachment (~11s).

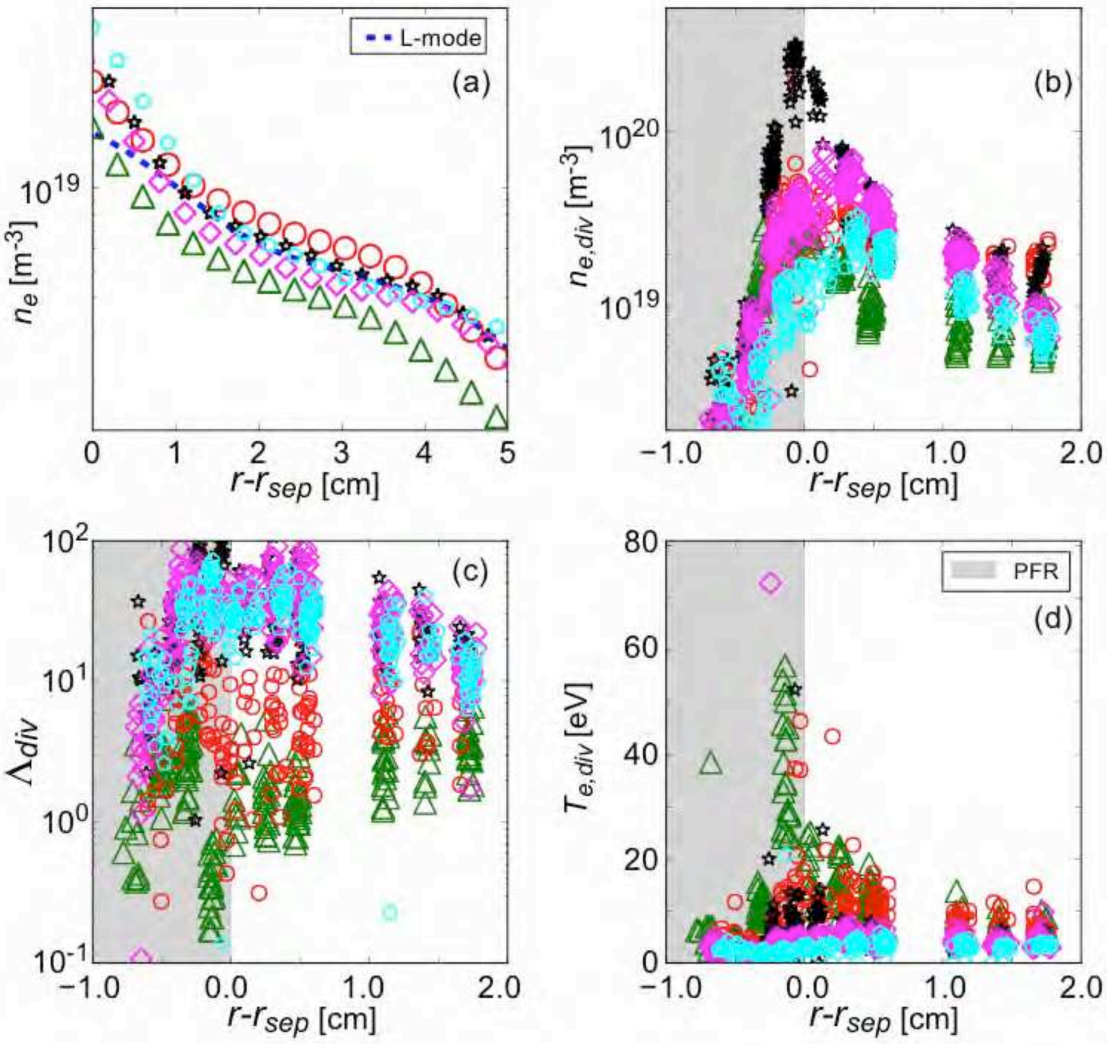

Figure 25: Upstream density profiles (a), divertor probe data (b,d) and Λ_{div} (c) for a horizontal target H-mode N seeding ramp (JPN 89241). Symbols correspond to shaded regions in figure 24. Density profiles in (a) are inter-ELM. Strongly detached conditions are achieved due to N_2 seeding, shown by substantial strike point density reductions shown in (b). Density profiles in (a) do not flatten with divertor detachment.